



**HAL**  
open science

## Tailoring the structure of casein micelles through a multifactorial approach to manipulate rennet coagulation properties

Fanny Lazzaro, Antoine Bouchoux, Jared Raynes, Roderick Williams, Lydia Ong, Eric Hanssen, Valérie Lechevalier-Datin, Stéphane Pezenec, Hyun-Jung Cho, Amy Logan, et al.

### ► To cite this version:

Fanny Lazzaro, Antoine Bouchoux, Jared Raynes, Roderick Williams, Lydia Ong, et al.. Tailoring the structure of casein micelles through a multifactorial approach to manipulate rennet coagulation properties. *Food Hydrocolloids*, 2020, 101, pp.105414. 10.1016/j.foodhyd.2019.105414 . hal-02373068

HAL Id: hal-02373068

<https://institut-agro-rennes-angers.hal.science/hal-02373068>

Submitted on 21 Dec 2021

**HAL** is a multi-disciplinary open access archive for the deposit and dissemination of scientific research documents, whether they are published or not. The documents may come from teaching and research institutions in France or abroad, or from public or private research centers.

L'archive ouverte pluridisciplinaire **HAL**, est destinée au dépôt et à la diffusion de documents scientifiques de niveau recherche, publiés ou non, émanant des établissements d'enseignement et de recherche français ou étrangers, des laboratoires publics ou privés.



Distributed under a Creative Commons Attribution - NonCommercial 4.0 International License

1 **Tailoring the structure of casein micelles through a multifactorial approach to manipulate**  
2 **rennet coagulation properties**

3

4 Fanny Lazzaro<sup>1,2\*</sup>, Antoine Bouchoux<sup>3</sup>, Jared Raynes<sup>4</sup>, Roderick Williams<sup>4</sup>, Lydia Ong<sup>5,6,7</sup>, Eric  
5 Hanssen<sup>6</sup>, Valérie Lechevalier<sup>1</sup>, Stéphane Pezennec<sup>1</sup>, Hyun-Jung Cho<sup>8</sup>, Amy Logan<sup>4</sup>, Sally  
6 Gras<sup>5,6,7</sup>, Frederic Gaucheron<sup>1</sup>

7

8 <sup>1</sup> STLO, Agrocampus Ouest, INRA, 35000, Rennes, France

9 <sup>2</sup> CNIEL, Paris, France

10 <sup>3</sup> TBI, Université de Toulouse, CNRS, INRA, INSA, Toulouse, France

11 <sup>4</sup> CSIRO Agriculture & Food, 671 Sneydes Road, Werribee, Victoria 3030, Australia

12 <sup>5</sup> Department of Chemical Engineering, The University of Melbourne, Parkville, Victoria 3010,  
13 Australia

14 <sup>6</sup> Advance Microscopy Facility, The Bio21 Molecular Science and Biotechnology Institute, The  
15 University of Melbourne, Parkville, Victoria 3010, Australia

16 <sup>7</sup> The ARC Dairy Innovation Hub, The University of Melbourne, Parkville, Victoria, 3110

17 <sup>8</sup> Biological Optical Microscopy Platform, University of Melbourne, Parkville VIC 3010, Australia

18 \* Corresponding author. STLO, Agrocampus Ouest, INRA, 65 rue de Saint-Brieuc 35000,  
19 Rennes, France. flazzaro@hotmail.fr

20

21 **Abstract:**

22 The properties of casein micelles are known to be affected by modifications to the environment,  
23 such as variations in pH or the addition of salts, yet the scientific literature typically considers the  
24 effects of one factor at a time, while in industrial processes, several modifications are performed  
25 simultaneously. The aim of this study was to assess the impact of multifactorial environmental  
26 modifications on the colloidal, structural and rennet coagulation properties of casein micelles in a  
27 simplified model system. A key finding was that dense regions (~ 20 nm in size) could be  
28 released from the casein micelle. The addition of NaCl and CaCl<sub>2</sub> had opposing effects, *i.e.*  
29 enhancing or limiting this micellar disruption, respectively. A decrease in pH had the strongest  
30 impact on the mineral balance, causing the colloidal CaP to solubilize and the micelle to swell.  
31 The rennet clotting time was impacted by variations in pH and NaCl content. Interestingly, a  
32 consideration of all three levels of casein micelle structure and their interactions was needed to  
33 explain variations in the firmness of rennet gels. This study illustrates the complex interplay of  
34 factors affecting micellar structure and improves our understanding of how micelles can be  
35 manipulated to control their properties.

36  
37 Keywords: casein micelle, rennet properties, internal structure, multifactorial modifications, small  
38 angle neutron scattering, cryo transmission electron microscopy

39

## 40 1 Introduction

41 In milk, casein proteins ( $\alpha_{s1}$ ,  $\alpha_{s2}$ ,  $\beta$  and  $\kappa$ ) and minerals (mainly calcium phosphate (CaP)  
42 nanoclusters) self-assemble to form a colloid referred to as the casein micelle. Electrostatic,  
43 hydrophobic and Van der Waals forces hold the different components together leading to a  
44 polydisperse population of particles 100 – 200 nm in diameter (Dalgleish & Corredig, 2012; Holt,  
45 Carver, Ecroyd, & Thorn, 2013; Holt, 2016; Holt & Horne, 1996; Horne, 2017; Thorn et al.,  
46 2005). There is a consensus that casein micelles are stabilized through electrostatic and steric  
47 repulsions due to the presence of a polyelectrolyte brush of  $\kappa$ -casein at the micellar surface (de  
48 Kruif, 1999; de Kruif & Zhulina, 1996; Tuinier & de Kruif, 2002). Despite extensive studies the  
49 internal structure of the casein micelle, *i.e.* the interactions between caseins and the minerals  
50 located within the colloid structure, is still under debate. The recent use of small angle X-ray and  
51 neutron scattering (SAXS and SANS, respectively) in parallel with cryo-transmission electron  
52 microscopy (cryo-TEM) has enabled questions around the internal structure to be partially  
53 answered, although without general agreement (Bouchoux et al., 2015; Bouchoux, Gésan-  
54 Guiziou, Pérez, & Cabane, 2010; Day, Raynes, Leis, Liu, & Williams, 2017; De Kruif, 2014;  
55 Ingham et al., 2015, 2016; Marchin, Putaux, Pignon, & Léonil, 2007; Pignon et al., 2004; Shukla,  
56 Narayanan, & Zanchi, 2009). An early model for the micelle structure was the submicelle model  
57 (Schmidt, 1982; Walstra, 1999), more recently a second model has proposed a more open  
58 structure composed of dense regions, water channels and CaP nanoclusters.

59 Environmental factors such as variations in pH, temperature and the addition of salts or  
60 chelating agents (de Kort, Minor, Snoeren, van Hooijdonk, & van der Linden, 2011; Gaucheron,  
61 2004; Lazzaro et al., 2017; Silva et al., 2013) induce shifts in the mineral balance between the  
62 diffusible and colloidal phases of the casein micelle. These mineral modifications also involve  
63 colloidal modifications that lead to changes in the functional properties of the casein micelle,  
64 such as the formation and stability of emulsions, thermal stability, and response to acid and  
65 rennet coagulation (Broyard & Gaucheron, 2015; Gaucheron, 2004). Although the mineral

66 fraction only represents a small proportion of the milk components (0.7%), it is used to control  
67 the properties of numerous manufactured dairy products.

68 The response of casein micelles to the addition of chymosin (rennet) and gelation is also of  
69 primary interest. For simplicity, the rennet coagulation mechanism applied to the micelles within  
70 many dairy ingredient streams can be divided into three steps: firstly, chymosin hydrolyzes  $\kappa$ -  
71 casein located at the surface of the casein micelle by cleaving the Phe(105)-Met(106) bond.  
72 Once sufficient  $\kappa$ -casein has been hydrolyzed, depleted micelles aggregate together, as  
73 described by many authors including Lucey and colleagues (Lucey, 2002), followed by a  
74 reorganization and reticulation to form the casein gel network structure (Dalglish & Corredig,  
75 2012). In reality this is continual process, and compositional factors such as changes in the fat or  
76 protein content (Guinee et al., 1997), pH (Mishra et al., 2005) or the addition of calcium  
77 (Udabage et al., 2001) can influence the onset and rate of gelation and the functionality of the  
78 resulting gel. Rennet coagulation can be assessed by two main characteristics: (i) the rennet  
79 clotting time (RCT), which quantifies the time elapsed from the addition of rennet or chymosin to  
80 the detectable onset of gelation, and (ii) the gel firmness. The RCT mainly depends on the rate  
81 of the enzymatic reaction and the aggregation of the para-caseinates (first and second steps),  
82 while the firmness depends on the organization and the strength of the resulting gel (third step).

83  
84 Variations in pH and the addition of NaCl and CaCl<sub>2</sub> are steps commonly applied to control the  
85 coagulation of milk. Many studies have been published describing the separate influence of each  
86 of these parameters on the colloidal properties and on the rennet coagulation properties of the  
87 casein micelle (Bulca, Wolfschoon-Pombo, & Kulozik, 2016; Choi, Horne, & Lucey, 2007;  
88 Daviau, Famelart, Pierre, Goudedranche, & Maubois, 2000; Deeth & Lewis, 2015; Famelart, Le  
89 Graet, & Raulot, 1999; Famelart, Lepesant, Gaucheron, Le Graet, & Schuck, 1996; Grufferty &  
90 Fox, 1985; Karlsson, Ipsen, & Ardö, 2007; Karlsson et al., 2007; Sandra, Ho, Alexander, &  
91 Corredig, 2012; Sbodio, Tercero, Coutaz, & Revelli, 2006; Zhao & Corredig, 2015; Zoon, van

92 Vliet, & Walstra, 1988, 1989). Although necessary to understand the dissociated effect of each  
93 parameter, this monofactorial approach does not correspond to the reality of the dairy industry  
94 where a multifactorial approach often occurs with the simultaneous variation of several  
95 parameters.

96 The aim of the current study was to investigate the effect of simultaneous modifications of the  
97 physico-chemical parameters on both the colloidal properties and the rennet induced  
98 coagulation of casein micelles in a simple model system, with a goal of better understanding the  
99 response of casein micelles to environmental changes. An experimental matrix of 27 different  
100 suspensions of casein micelles in non-native conditions within water, with variations in added  
101 NaCl and CaCl<sub>2</sub>, at three different pH was designed. A combination of multiple advanced  
102 biophysical techniques, such as cryo-TEM and SAXS, was used to make a thorough  
103 characterization of the casein micelles in terms of physicochemical, structural and renneting  
104 properties. Appropriate statistical analyses were applied to establish the relationships between  
105 the colloidal and the rennet coagulation properties of the modified casein micelles, leading to the  
106 first study that combines SAXS characterization with an assessment of the functional properties  
107 of casein micelles.

108

## 109 **2 Materials and methods**

### 110 **2.1 Chemicals**

111 All chemicals used for this study, hydrochloric acid (VWR chemicals, Fontenay-sous-bois,  
112 France), NaCl (PanReac AppliChem, Barcelona, Spain), CaCl<sub>2</sub> (VWR International, Leuven,  
113 Belgium) and sodium azide (Riedek-de Haën, Seelze, Germany) were of analytical grade.

### 114 **2.2 Materials**

115 Experiments were carried out using a native phosphocaseinate (NPC) powder resuspended in  
116 deionised water at  $24.2 \pm 0.8$  g kg<sup>-1</sup> of protein. Concentrated NPC was supplied by Gillot SAS  
117 (Saint Hilaire de Briouze, France) and obtained by microfiltration (0.1 µm pore size membrane)

118 of raw skimmed milk followed by diafiltration against milli-Q water. The concentrate was then  
119 spray dried according to the method described by Pierre, Fauquant, Le Graet, & Maubois (1992)  
120 and Schuck et al., (1994) using Bionov facilities (Rennes, France). Casein and their associated  
121 minerals represented more than 90% of the total solid content of the powder. Residual whey  
122 proteins (3%) (w/w) and traces of lactose were present in the powder.

123 For the coagulation experiments, Chr. Hansen (Hoersholm, Denmark) supplied commercial  
124 chymosin (CHY-MAX M 200, 200 IMCU ml<sup>-1</sup>).

### 125 **2.3 Preparation of casein micelle suspensions**

126 An experimental matrix was designed to assess the concomitant effects of variations in pH and  
127 the addition of NaCl or CaCl<sub>2</sub>. The range of pH and the final concentrations of added NaCl and  
128 CaCl<sub>2</sub> were selected to produce suspensions which would form gels within one hour after the  
129 addition of a set amount of chymosin. The pH values targeted were 5.7, 6.3 or 6.9 and the final  
130 concentrations of NaCl and CaCl<sub>2</sub> in the suspensions were 0, 50 and 100 mmol kg<sup>-1</sup> or 0, 7.5 and  
131 15 mmol kg<sup>-1</sup>, respectively. A full experimental design was carried out, where 27 different  
132 suspensions of casein micelles were prepared in water, with different salt and pH environments.  
133 The suspensions were named from A to Z, and CTRL to represent the control which consisted of  
134 NPC in water at pH 6.9, with no added salts (Fig.1).

135 Dispersion of the NPC powder in milli-Q water was performed as described in Lazzaro et al.,  
136 (2017). Briefly, the powder was stirred (900 rpm) at 40 °C for 6 h, followed by an additional 16 h  
137 at room temperature overnight. The proper resuspension of the ingredient was checked by laser  
138 light diffraction according to Schuck, Dolivet, & Jeantet (2012), ensuring the proportion of  
139 insoluble particle was below 10 %. Varying amounts of stock solutions of NaCl (2.5 mol kg<sup>-1</sup> in  
140 milli-Q water, pH 6.9) and CaCl<sub>2</sub> (0.25 mol kg<sup>-1</sup> in milli-Q water, pH 6.9) were added to the  
141 concentrated suspensions of NPC in milli-Q water with stirring to reach the required salt  
142 concentration. The pH shift induced by the addition of salts was corrected using HCl 1M in milli-  
143 Q water and set to 5.7, 6.3 or 6.9. The suspensions were then diluted to 24.2 ± 0.8 g kg<sup>-1</sup> of

144 protein and left overnight at room temperature. If necessary, the pH was readjusted prior to  
145 experiments. For convenience, Tables 1, 2, 3 and Figures 6, 7, 8 report the results of different  
146 analyses for a set on 9 samples only. These selected samples correspond to the corners of the  
147 cubic experimental design (suspensions A, B, D, E, J, L, M, CTRL ; extreme points) and the  
148 center point of the experimental design (suspension T) (Fig. 1).

## 149 **2.4 Recovery of the diffusible phases of the suspensions**

150 Aliquots (15mL) of each NPC suspension were ultrafiltered by centrifugation for 30 min, at 20°C  
151 and 1800 *g*. using Vivaspin concentrators (molecular weight cut-off 10 kDa, Vivascience,  
152 Palaiseau, France). The diffusible phases were analyzed to determine the concentrations of  
153 diffusible ions and used for the dilution of the suspension for the turbidity ( $\tau$ ) and nanoparticle  
154 tracking analysis (NTA) measurements and for the background determination for the SAXS  
155 measurements.

156

## 157 **2.5 Analysis**

### 158 **2.5.1 Protein content**

159 The total nitrogen content of each suspension was determined according to the Kjeldahl method  
160 (IDF standard 20-1, 2014). A factor of 6.38 was used to convert nitrogen to protein  
161 concentration. Measurements were performed in duplicate.

### 162 **2.5.2 Mineral composition and distribution**

163 Total and diffusible cations (calcium Ca, sodium Na) and anions (chloride Cl, inorganic  
164 phosphate Pi) contents were determined as described in Lazzaro et al., (2017). Colloidal  
165 concentrations were deduced by subtracting the concentration of diffusible ions from the  
166 concentration of total ions. The mineral concentrations were adjusted to account for the small  
167 differences in protein content (see section 2.5.1.).

### 168 **2.5.3 Turbidity measurements**

169 Absorbance measurements were carried out at 600 nm and 20 °C using a UV-visible  
170 spectrometer (UVmc<sup>2</sup>, Safas, Monaco). The casein micelle suspensions were diluted 10 times in  
171 their diffusible phases and analyzed immediately. The diffusible phase for each suspensions  
172 was also analyzed. Absorbance measurements were converted into turbidity ( $\tau$ ) according to the  
173 following formula:

$$174 \quad \tau = 2.303 * \frac{OD(600nm)}{l} \quad (1)$$

175 with  $OD(600nm)$  being the optical density of the suspension (difference between the absorbance  
176 of the diluted suspension and the absorbance of its diffusible phase) ; and  $l$  the light path length  
177 ( $l = 1 \text{ cm}$ ).

#### 178 **2.5.4 Nanoparticle tracking analysis**

179 Nanoparticle Tracking Analysis (NTA) was performed at 20 °C using a Nanosight NS300  
180 (Malvern Instruments, Malvern, United Kingdom) equipped with a Nanosight syringe pump. The  
181 principle of NTA is based on the tracking of individual particles in suspension. A large dilution  
182 (40,000 times) of the casein micelle suspension in their own diffusible phase was necessary to  
183 meet the optimal settings of the apparatus, *i.e.* 20 – 100 particles per frame during the  
184 measurement combined to a dark background image. A syringe was loaded with the diluted  
185 suspension and the focus adjusted manually. The infusion rate was set to 20, the camera level  
186 to 12 and 5 video images of 60 s each were recorded. The video images of the movement of  
187 particles under Brownian motion were analyzed by the NTA image analysis software (V 3.0  
188 0064., Malvern Instruments). The minimum screen gain, and detection threshold of 3 were  
189 selected to maximize the detection of small particles (< 50 nm diameter). The particle size  
190 distributions obtained (data not shown) were fitted with a log-normal population of particles using  
191 Schulz equation (Schulz, 1935):

$$192 \quad W(R, r_{NTA}, \sigma) = \frac{R^Z}{\Gamma(Z+1)} \left( \frac{Z+1}{r_{NTA}} \right)^{Z+1} \times \exp \left[ -\frac{R}{r_{NTA}} (Z + 1) \right] \quad (2)$$

193 Where  $r_{NTA}$  is the average radius of the particles and Z relates to the polydispersity ( $\sigma$ ) of the  
194 particle radii (R) given by the expression:

$$195 \quad \sigma = \left( \frac{\overline{R^2}}{r_{NTA}^2} - 1 \right) = \frac{1}{Z+1} \quad (3)$$

196 The value of  $\sigma$  varied from 0.23 to 0.47 within the set of suspensions and  $r_{NTA}$  was further used  
197 in the statistical analyses.

### 198 **2.5.5 Cryogenic Transmission Electron microscopy**

199 A thin vitrified film of casein micelle suspension was prepared as described in the method of  
200 Chen et al., (2011). A Formvar lacey carbon film mounted on a 300 mesh copper grids  
201 (ProSciTech, Queensland, Australia) were glow discharged for 15 s and used as a hydrophilic  
202 support on which the suspensions (4  $\mu$ L) were adsorbed. After 30 s, the grids were plunged in  
203 liquid ethane using a Vitrobot (FEI Company, Eindhoven, Netherlands) to freeze the sample.  
204 The grids were observed on a Technai G2 TF30 (FEI company, Eindhoven, Netherlands)  
205 operating at 200 kV and equipped with a Gatan US1000 2kX2k CCD Camera (Gatan). Between  
206 10 and 20 micrographs per suspension were recorded under low-dose conditions with defocus  
207 values of 4 - 6  $\mu$ m. Image analysis was performed using Image J software (National Institute of  
208 Health, USA). Due to the large numbers of samples, this process was automated through the  
209 use of macros set up within Image J. In total, between 1,554 particles (in suspension TEM) and  
210 29,092 particles (in suspension B) were measured in three steps:

211 i) The region of interest (ROI) was defined:

212 Particle detection was strictly limited to the area free from the grid structure and ice particles  
213 present as a result of sample preparation.

214 ii) Particle detection:

215 To detect particles, the background was subtracted from images using a 'rolling ball' algorithm  
216 and smoothed using Gaussian filtering before the threshold was applied and particles measured.

217 Touching particles were separated using the distance transform watershed plugin (Quasi-

218 Euclidean). Most of the very large particles (diameter > 50 nm) were often partially hidden by the  
219 grid. Therefore, the grid-obstructed particles were excluded from the detection only if more than  
220 10% of the area defined by the best-fitted ellipse drawn around the particle was hidden under  
221 the grid. In order to prevent any misrepresentative segmentation, which can be caused from  
222 automatic detection, all segmentation results were visualized and the overlay was saved as a  
223 separate image that was manually inspected.

224 iii) Shape measurement of the particles:

225 Feret's diameter was determined for each particle detected. Particles were defined as small (<  
226 50 nm in Feret's diameter) or large (> 50 nm in Feret's diameter). The ratio of small to large  
227 particles was then calculated for each suspension and defined as  $\Gamma_{s/l}$ .

## 228 **2.5.6 Small angle X ray scattering measurements, data treatment and modelling**

229 The SAXS measurements were carried out on the suspensions and their respective diffusible  
230 phases at the SAXS/WAXS beamline of the Australian Synchrotron (Clayton, Melbourne,  
231 Australia). The beamline is equipped with a Pilatus 1 M detector (170 mm x 170 mm, effective  
232 pixel size of 172 x 172  $\mu\text{m}$ ). Each sample was measured at sample-to-detector lengths of 7.106  
233 m and 0.721 m with respective photon energies of 8.2 keV (1.512  $\text{\AA}$ ) or 18.1 keV (0.685  $\text{\AA}$ ).  
234 Merging the data from both distances provided a  $q$  range of  $1.3 \times 10^{-3}$  to  $1.93 \text{\AA}^{-1}$ . The samples  
235 were drawn into a 1.5 mm glass capillary; allowing continuous flow through the X-ray beam  
236 during measurements. The data were obtained from at least 10 exposures of 2 s intervals at  
237 20°C. The capillary was rinsed with water, followed by 8 M guanidine and again with water  
238 before being air-dried between each sample analysis.

239 The SAXS intensities were normalized to an absolute scale and at least 10 measurements per  
240 sample were averaged to obtain the intensity profiles using ScatterBrain (V 2.71) (Australian  
241 Synchrotron, Clayton, Australia). Measurements of the diffusible phases for each suspension  
242 were subtracted from the corresponding scattering intensities of the suspensions to account for  
243 background. Finally, the intensities were adjusted to account for the difference in total protein

244 content of the suspensions in Primus (V 3.2) (ATSAS, Hamburg, Germany). Igor software (V  
245 7.0.2.2) (Wave Metrics, Lake Oswego, USA) was used to merge the data from the 7.106 and  
246 0.721 m detector distances to obtain the final curves  $I = f(q)$ .

247 The SAXS scattering intensity curves were fitted according to the model of Bouchoux et al.,  
248 (2010) with slight modifications. This model considers three populations of particles: Population  
249 A, observed at low  $q$  (up to  $6 \times 10^{-3} \text{ \AA}^{-1}$ ) where the scattering intensity corresponds to the  
250 presence of casein micelles; population B, in the intermediate  $q$  regions ( $6 \times 10^{-3}$  to  $2 \times 10^{-2} \text{ \AA}^{-1}$ ),  
251 where the scattering corresponds to dense regions inside the casein micelles and population C;  
252 at high  $q$  ( $7-8 \times 10^{-2} \text{ \AA}^{-1}$ ) attributable to the CaP nanoclusters. The intensity depends on the form  
253 factor of each population  $P_n(q)$  (approximated by the form factor of polydisperse spheres of  
254 mean radius  $r_a$ ,  $r_b$  and  $r_c$ ) and on prefactors  $a$ ,  $b$  and  $c$ :

$$255 \quad I(q) = a P_a(q) + b P_b(q) + c P_c(q) \quad (4)$$

256 with:

$$257 \quad a = \alpha \times n_a (Vma \times \Delta\rho_a)^2 \quad (5)$$

$$258 \quad b = \alpha \times n_b (Vmb \times \Delta\rho_b)^2 \quad (6)$$

$$259 \quad c = \alpha \times n_c (Vmc \times \Delta\rho_c)^2 \quad (7)$$

260 where  $n_a$ ,  $n_b$ ,  $n_c$  were the number of scatterers for each population,  $Vma$ ,  $Vmb$ ,  $Vmc$  their volume  
261 and  $\Delta\rho_a$ ,  $\Delta\rho_b$ ,  $\Delta\rho_c$  their contrast, respectively.

262 The absolute number of casein micelles was assumed to be the same in all the suspensions.  
263 This hypothesis is based on the observations of Moitzi, Menzel, Schurtenberger, & Stradner,  
264 (2011) that a decrease in pH left the number of casein micelles unmodified, even if some casein  
265 micelle materials are subdivided into individual monomers or smaller casein aggregates with a  
266 resulting decrease in micelle size and mass. In the present study, it was also assumed that the  
267 modifications of the pH and the addition of NaCl and CaCl<sub>2</sub> applied in the experimental design  
268 were not sufficient to cause the complete disruption of the micellar structure. This implies that  
269 the  $n_a$  value is not affected by the physical-chemical modifications of our samples. We chose to

270 set it  $n_a$  to 1 so that  $n_b$  and  $n_c$  are defined relative to a singular casein micelle. As a  
271 consequence, the constant  $\alpha$  accounts for both the electron scattering length and the absolute  
272 number density of casein micelles in the samples.

273 This model was tested on our data according to the procedure of Bouchoux et al., (2010). First,  
274 the value of the radius of each population,  $r_a$ ,  $r_b$  and  $r_c$ , and the prefactors,  $a$ ,  $b$ ,  $c$ , were  
275 determined by fitting the model to the experimental data with polydispersities set to  $\sigma_a = 1/3$ ,  $\sigma_b =$   
276  $1/3$  and  $\sigma_c = 0.2$ . The good quality of the fits support the value of polydispersity used in this  
277 study to describe scattering that relates to casein micelle size. Note that we decided not to use  
278 the polydispersity values determined by NTA (2.5.4) given that the SAXS and the NTA methods  
279 cover different size ranges for the assessment of the physical properties of the particles in  
280 suspension.

281 In a second step, the value of the constant  $\alpha$  was calculated from the control sample (CTRL)  
282 using the prefactor  $a$  obtained from the fit, the size (and therefore volume) of the micelle in this  
283 case, and the contrast  $\Delta\rho_a$  of a native casein micelle in water, *i.e.*  $0.018 \text{ e- \AA}^{-3}$  ( $\rho_{\text{water}} = 0.334 \text{ e-}$   
284  $\text{\AA}^{-3}$  and  $\rho_{\text{caseinmicelle}} = 0.352 \text{ e- \AA}^{-3}$ ).

285 In a third step, the values of  $\Delta\rho_a$ ,  $n_b$  and  $n_c$  were calculated for the 27 suspensions using the  
286 sizes and prefactors obtained from the fits. The micelle,  $\Delta\rho_a$  was simply calculated from  
287 prefactors  $a$  and sizes  $r_a$ , knowing that  $n_a = 1$ . The number of dense regions  $n_b$  was calculated  
288 from prefactors  $b$ , sizes  $r_b$ , and making the assumption that contrast  $\Delta\rho_b$  is relatively insensitive  
289 to the physical-chemical modifications performed in this study.  $\Delta\rho_b$  is taken as  $0.035 \text{ e- \AA}^{-3}$ , *i.e.*  
290 twice the contrast of the micelle assuming that dense regions occupy 50% of the total volume of  
291 the casein micelle (Bouchoux et al. 2010). The CaP nanoclusters / Protein inhomogeneities,  $n_c$   
292 was calculated from prefactors  $c$ , sizes  $r_c$ , and an estimated contrast  $\Delta\rho_c$  of  $0.172 \text{ e- \AA}^{-3}$  that was  
293 also assumed to be constant between samples. Note that in a recent work, Ingham et al., (2016)  
294 suggest a new interpretation and assign the high  $q$  features of SAXS data to the presence of  
295 inhomogeneous protein structures of 1-3 nm length scale instead of CaP nanoclusters. As our

296 purpose is not to take a position on this question, we decided not to restrict our analysis solely to  
297 the interpretation of Bouchoux et al. (2010). A number of possible inhomogeneities  $n_{cPI}$  was  
298 therefore calculated following Ingham's postulate, this time using an estimated contrast of 0.126  
299  $e^{-\text{Å}^{-3}}$  (Ingham et al., 2016).

### 300 **2.5.7 Rennet coagulation properties**

301 The coagulation properties of samples were assessed using a ChymoGRAPH® (Chr Hansen,  
302 Denmark) which uses a similar physical principal to the Formagraph (McMahon & Brown, 1982)  
303 and where coagulation is determined according to the movement of a stainless steel, loop  
304 pendulum immersed in the samples. Casein micelles suspensions (10 g) were weighed into the  
305 wells of the ChymoGRAPH® stainless steel block which was immersed in a water bath for 10  
306 min to equilibrate the temperature of the block and suspension to 30°C. A sample of 400  $\mu\text{L}$  of  
307 the enzyme solution (chymosin diluted ten times in milli-Q water) was added and the  
308 suspensions, stirred for 30 s with the spoons and transferred from the water bath to the  
309 oscillating plate. A Peltier module maintained the temperature of the block at 30°C. When the  
310 coagulation began, the resulting increase in viscosity and the formation of gels caused the  
311 pendulums to oscillate together with the samples. The movement of each pendulum was  
312 measured by the use of optical fibers over a period of 60 min and the data collected using the  
313 ChymoGRAPH® software (V 1.0, Chr Hansen, Denmark). The RCT corresponded to the time  
314 elapsed from chymosin addition to the detectable onset of gelation, where gelation was defined  
315 as at the time point when the firmness of the suspensions was  $> 0$ . The maximal firmness  
316 recorded during the 60 min duration of the experiment was defined as the firmness of the gel.

### 317 **2.5.8 Statistical treatments**

318 As mentioned in section 2.3., a complete experimental design was carried out to study the  
319 combined effects of variation in pH (5.7, 6.3, 6.9), NaCl addition (0, 50, 100  $\text{mmol kg}^{-1}$ ) and  
320  $\text{CaCl}_2$  addition (0, 7.5, 15  $\text{mmol kg}^{-1}$ ) on the colloidal and renneting properties of the casein  
321 micelles (Fig. 1).

322 The data set was subjected to principal component analysis (PCA) to highlight relationships  
323 between measured variables, and similarities between samples. The general purpose of PCA is  
324 to summarize a data set with an optimized, controlled loss of information (Jolliffe, 1986; Abdi &  
325 Williams, 2010). It allows one to identify patterns which are the most representative of the  
326 variability in the whole data set, and to locate individual samples on similarity maps based on  
327 these patterns.

328 If the data consist in  $p$  variables measured for each of the samples, any sample may be  
329 represented as a point in a  $p$ -dimensional space. Then, PCA can be viewed as the projection of  
330 the data on a subspace which maximizes the dispersion of the projected data (variance  
331 maximization). The axes that define this subspace, are new variables, called principal  
332 components, which are linear combinations of the  $p$  initial variables. They are orthogonal (thus  
333 uncorrelated) and ordered by decreasing projected variance, in such a way that the few first  
334 principal components account together for the most part of the variability (the "information") in  
335 the data set. For each principal component, the coefficients for the  $p$  initial variables (called  
336 "loadings") illustrate their respective contributions in the principal component, and are used to  
337 interpret the physical meaning of the new variable. Each sample is then characterized by the  
338 respective values taken by these new variables, called the scores of the sample on the different  
339 principal components. These scores represent the coordinates of each sample on a factorial  
340 map, whose axes origin corresponds to the average spectrum.

341 PCA was performed after variable centering and scaling to unit variance using the R software  
342 package (R Core Team, 2018) and the FactoMineR package (Lê, Josse, & Husson, 2008). All  
343 the correlations mentioned in the results and discussion section were found to be significant ( $p <$   
344  $0.05$ ) using the paired student  $t$ -test.

345 In addition, multiple linear regression was also applied to the SAXS variables  $r_a$ ,  $n_b$  and  $n_{CaP}$ ,  
346 using the software STATGRAPHICS Centurion XVII (V. 17.1.10, Statpoint Technologies, The  
347 Plains, USA) in order to evaluate the effect of these structural features on the firmness of the

348 gel. A model of firmness was defined that included the quadratic effects of  $r_a$ ,  $n_b$  and  $n_{cCaP}$  and  
349 the second order interactions between these factors. The full equation of the model was:

$$350 \text{ Firmness} = \text{constant} + r_a + n_b + n_c + r_a^2 + n_b^2 + n_c^2 + (r_a \times n_b) + (r_a \times n_c) + (n_b \times n_c)$$

351 (8)

352 The LS-means were calculated and differences regarded as significant for  $p < 0.05$ . Non-  
353 significant effects were excluded from the model, except when first order effects were  
354 participating in interaction effects.

355

### 356 **3 Results and discussion**

357 The experimental protocol applied in this study allowed the effect of variations in added NaCl  
358 and  $\text{CaCl}_2$  on the colloidal properties and gelation properties of the casein micelle to be  
359 examined. Analysis was performed at three different pH, and conditions for each suspension  
360 were non-native and carefully controlled, to allow for compositional structure-function effects to  
361 be isolated.

362 The results of the biophysical analyses are presented and discussed in two main sections. In the  
363 first section, the PCA analyses are used to (i) assess the impacts of variation in pH and the  
364 addition of NaCl and  $\text{CaCl}_2$  on the mineral balance of the casein micelle, (ii) establish  
365 relationships between the structure of the casein micelle and its other colloidal properties. In the  
366 second section, the relationships between rennet coagulation properties and colloidal and  
367 structural features of casein micelle are considered. For these experiments rennet is added to  
368 induce coagulation, but no starter culture is added to simplify the model experimental system  
369 examined. PCA analyses were able to explain the variation observed in RCT, while linear  
370 regression is able to explain interactions between the structural properties and the firmness of  
371 the rennet gels.

#### 372 **3.1 Colloidal and structural properties of the modified casein micelles**

373 In the general case, the output of PCA is dual: it consists numerically in i) the loadings of the  
374 initial variables in each of the principal components, which illustrate the main dimensions of  
375 variability in the data set, and ii) the scores of the samples on the principal components, *i.e.* their  
376 coordinates on similarity maps.

377 It was found that almost 80 % of the variability (total variance) observed within our experimental  
378 design is accounted for together by the first four principal components (34.4 %, 23.5 %, 11.2 %  
379 and 10.1 %, respectively). To illustrate the respective contributions of the initial variables to  
380 principal components, one may use correlations between initial variables and principal  
381 components, *e.g.* as in Fig. 2 and Fig. 4.

382 As a rule of interpretation and for example, PC1 is highly positively correlated with colloidal Ca,  
383 while PC2 is highly positively correlated with diffusible Na (Fig. 2). Any sample with a high  
384 positive score on PC1 (PC2, respectively) would then be characterized by a high content in  
385 colloidal Ca (diffusible Na, respectively).

### 386 **3.1.1 Impact of the environmental modifications on the mineral balance of the casein** 387 **micelle**

388 Analysis of the partition of minerals Ca, Pi, Na and Cl between the colloidal and diffusible  
389 phases of the suspensions (Table 1) revealed that the colloidal ions consisted mainly in Ca and  
390 Pi, whereas Na and Cl were mainly present in the diffusible phases of the suspensions when  
391 NaCl was added. Figure 2 shows the strong, positive correlations between the pH and colloidal  
392 Ca and Pi (0.85 and 0.80, respectively) and a negative correlation with the concentration of  
393 diffusible Pi (- 0.86). The diffusible Ca concentration was weakly, but still significantly, impacted  
394 by variation in pH, with a correlation coefficient of - 0.5 (Fig. 3).

395 The strongest variation of Ca in the diffusible phase was attributed to the addition of CaCl<sub>2</sub>, with  
396 a correlation coefficient of 0.84 (Fig. 4). Colloidal and diffusible concentrations of Pi were also  
397 significantly impacted by the addition of CaCl<sub>2</sub> but to a much smaller extent, with correlation  
398 coefficients of 0.42 and - 0.42 respectively (Fig. 3). These results confirm that modifications in

399 pH and CaCl<sub>2</sub> induced opposite effects on the mineral content of the casein micelle, with pH  
400 inducing a stronger effect compared to CaCl<sub>2</sub> addition.

401 A decrease in pH led to the solubilization of the CaP nanoclusters, which has been reported in  
402 the literature (Dalglish & Law, 1989; Daviau, Famelart, Pierre, Goudrdranche, & Maubois,  
403 2000; Famelart, Lepesant, Gaucheron, Le Graet, & Schuck, 1996; Le Graet & Brulé, 1993; Le  
404 Graet & Gaucheron, 1999; Le Ray et al., 1998; van Hooydonk, Boerrigter, & Hagedoorn, 1986;  
405 Zoon, van Vliet, & Walstra, 1989). Conversely, the addition of CaCl<sub>2</sub> limited CaP solubilization  
406 presumably by shifting the Ca<sup>2+</sup> equilibrium through the saturation of the diffusible phase (Moitzi  
407 et al., 2011). Added Ca would also directly associate with caseins and/or with the diffusible Pi  
408 and precipitate as CaP (Le Ray et al., 1998; Philippe, Le Graet, & Gaucheron, 2005; Philippe,  
409 Gaucheron, Le Graet, Michel, & Garem, 2003; Udabage, McKinnon, & Augustin, 2000).

410 The addition of NaCl positively correlated with the diffusible Na and Cl concentrations (0.99 and  
411 0.95, respectively) (Fig. 2), which was consistent with the presence of NaCl in the diffusible  
412 phase. No significant correlation was found between NaCl addition and the concentrations of  
413 colloidal ions (Fig. 2) *i.e.* NaCl had no direct effect on the mineral content of the casein micelle  
414 within the range studied (0 to 100 mmol kg<sup>-1</sup>). This result is in agreement with the finding of  
415 Karlsson, Ipsen, & Ardö (2007) who reported no change in the colloidal CaP content. However,  
416 this observation differs from the results of Aoki, Umeda, & Nakao, (1999); Famelart et al.,  
417 (1996); Grufferty & Fox, 1985; Zhao & Corredig, (2015); Zoon et al., (1989) who reported that  
418 solubilization of Ca, and occasionally Pi, occurred when NaCl was added to fresh or  
419 reconstituted skim milk or casein micelle suspensions. These discrepancies could arise from  
420 differences in pH, as in most cases, variations in pH induced by NaCl addition were not  
421 corrected, and/or the amount of added NaCl was 3 to 5 times higher than in the present study.

422 **3.1.2 Consequences on the structural properties of the casein micelle**

423 The SAXS data presented in Fig. 5 were treated primarily using the sponge-like model defined  
424 by Bouchoux, Gésan-Guiziou, Pérez, & Cabane, (2010) which uses three populations to

425 interpret the SAXS pattern of casein micelles. The alternate interpretation of Ingham et al.,  
426 (2016) also defines three population but attributes population C; at high  $q$  ( $7-8 \times 10^{-2} \text{ \AA}^{-1}$ ), to  
427 protein inhomogeneties rather than the CaP nanoclusters. Given that we have decided not to  
428 rely exclusively on the interpretation of either Ingham et al., (2016) or Bouchoux et al., (2010),  
429 the implications of both studies are discussed here. The SAXS patterns (Fig. 5) show variability  
430 in the intensity of signal across these 3 different regions for the set of 9 selected samples. The  
431 structural features determined from the SAXS data ( $r_a$ ,  $\Delta\rho_a$ ,  $r_b$ ,  $n_b$ ,  $r_c$ ,  $n_c$ ) for the 27 suspensions  
432 were compared to the other physico-chemical variables (*e.g.* concentrations of colloidal and  
433 diffusible minerals,  $\tau$ ,  $r_{\text{nano}}$ ,  $\Gamma_{\text{s/l}}$ ) for each population of scatterers (A, B and C) and analysed by  
434 PCA (Figs. 2, 3, 4). These correlations and the relevance of the two SAXS models applied are  
435 discussed in the following sections.

#### 436 **3.1.2.1 Population A: the casein micelle**

437 The modelling of the SAXS data enabled 2 variables,  $r_a$  and  $\Delta\rho_a$ , describing the casein micelle  
438 radius and its contrast to be defined, respectively. The radius,  $r_a$  varied from 41.5 to 58.1 nm  
439 (Table 2), which is consistent with values determined in earlier characterizations of milk or  
440 casein micelle dispersions by SAXS (Bouchoux et al., 2010; Ingham et al., 2016; Pignon et al.,  
441 2004; Shukla et al., 2009). Moreover,  $r_a$  positively correlated with the mean micellar radius  
442 measured by NTA,  $r_{\text{NTA}}$  ( $53.8 < r_{\text{NTA}} < 74.8 \text{ nm}$ ) of the different suspensions (Fig. 2 and Table 2),  
443 with a correlation coefficient of 0.72. **These size measurements are close to those for native**  
444 **casein micelles in milk measured by NTA (Priyashantha et al. 2019).**

445 The PCA also suggests a dependency between the micellar size and mineral balance. Indeed,  $r_a$   
446 showed negative correlations with colloidal concentrations of Ca and Pi (- 0.71 and - 0.38,  
447 respectively) and a positive correlation with the concentration of diffusible Pi (0.38) (Fig. 2). The  
448 solubilization of the micellar CaP caused by a decrease in pH resulted in an increase in micellar  
449 size due to swelling. This size increase also affected the turbidity of the suspensions that  
450 increased (correlation coefficient of - 0.46 between pH and  $\tau$ ) (Fig. 2). These results were in

451 agreement with those of Daviau et al., (2000) and van Hooydonk et al., (1986) but differed to the  
452 observations of Moitzi et al., (2011) and Ouanezar, Guyomarc'h, & Bouchoux, (2012). These  
453 last authors reported a decrease of micellar diameter, measured by multiple angle 3D light  
454 scattering or by AFM microscopy, respectively. In these studies, skim milk and casein micelle  
455 powders were resuspended in deionised water or synthetic milk ultrafiltrate (lactose free saline  
456 solution), respectively, providing a different ionic environment for the casein micelles than in our  
457 study. In addition, the pH ranges covered in these studies were lower than herein, possibly  
458 leading to differences in behavior when the colloid is exposed to more severe conditions.  
459  $\text{CaCl}_2$  addition had no impact on  $r_a$  (Fig. 3), which was in agreement with results reported by  
460 Philippe et al., (2005); Philippe et al., (2003) and Udabage et al., (2000). Conversely, the  
461 concentrations of NaCl and diffusible Na significantly correlated with  $r_a$  (- 0.46, - 0.43,  
462 respectively) (Fig. 2), with NaCl addition slightly reducing the diameter of the casein micelle. This  
463 differs from the findings of Zhao & Corredig, (2015) and Karlsson, Ipsen, Schrader, & Ardö,  
464 (2005), where an increase in the size of casein micelles was observed. It is possible, however,  
465 that in these previous studies, the increase in size was due to the decrease in pH (not corrected)  
466 induced by NaCl addition rather than the direct effect of the soluble NaCl salt. Here,  $\tau$  negatively  
467 correlated with NaCl (- 0.46) (Fig. 2), reflecting a decrease in scattering following NaCl addition.  
468 This result was in accordance with the two studies cited above and could be caused by a  
469 decrease in micellar size and/or internal rearrangements of the micelle structure. Diffusible Na  
470 may screen the negative charge on  $\kappa$ -casein CMP, causing a partial collapse of the hairy layer  
471 and a slight decrease in micellar size. The impact of NaCl on the size and turbidity of the casein  
472 micelles could also be related to the release of small casein aggregates (dense regions) from  
473 casein micelles. This argument is developed further in section 3.1.2.2 of the present paper.  $\Delta\rho_a$ ,  
474 defined as the contrast of the casein micelle, corresponds to the electron density of the micelle  
475 ( $\rho_{CM}$ ) relative to the electron density of the diffusible phase ( $\rho_{DF}$ ), which consists of water  
476 containing ions (Ca, Na, Cl and Pi) from the NPC powder and/or the addition of NaCl and  $\text{CaCl}_2$ .

477 The contribution of these diffusible ions to  $\rho_{DF}$  ranged from 0.02 to 0.73 %, and thus, was not  
478 taken into account here and  $\rho_{DF}$  was considered constant and equal to the electron density of  
479 water, ( $0.334 \text{ e}^- \text{ \AA}^{-3}$ ). Therefore, in the present study,  $\Delta\rho_a$  directly reflected the variation of the  
480 electron density of the casein micelle. This value depended on the volume, the casein  
481 concentration and the CaP content of the casein micelles.  $\Delta\rho_a$  varied between 0.010 and 0.018  
482  $\text{e}^- \text{ \AA}^{-3}$  (Table 2), which is of same order of magnitude as the contrast of a native casein micelle  
483 described by Bouchoux et al., (2010) and Ingham et al., (2016).  $\Delta\rho_a$  presented a negative  
484 correlation (-0.86) with  $r_a$  (Fig. 2). It also positively and strongly correlated with concentrations of  
485 colloidal Ca and Pi (0.90 and 0.67, respectively) (Fig. 2). These results were consistent with an  
486 increase in the volume of the casein micelle due to a depletion in CaP, leading to a decrease in  
487 the electron density of the micelle.

### 488 **3.1.2.2 Population B: the dense regions**

489 The scattering caused by population B is characterized by  $r_b$ , the radius, and  $n_b$ , the number of  
490 dense regions per casein micelle. Both features showed variability within the full sample set, with  
491 RSD's of 38.9 and 84.1 %, respectively (Table 2). PCA analysis (Fig 2.) indicates a strong and  
492 positive correlation (0.73) between  $n_b$  and  $\Gamma_{s/l}$ , the ratio of small (< 50 nm in Feret's diameter) to  
493 large (> 50 nm in Feret's diameter) particles detected on cryo-TEM micrographs (section 2.5.5)  
494 (Fig. 6).

495 Large black and homogeneous strands crossing the cryo-TEM micrographs (Fig. 6) correspond  
496 to the grids that support the suspensions and large circular spots (*e.g.* suspension E) or merged  
497 spots (*e.g.* suspension D) were individual casein micelles and aggregates of casein micelles,  
498 respectively. Differences in the granularity of the background of the images were attributed to  
499 the presence of small-dissociated aggregates of the casein micelle that were present in the  
500 diffusible phase. This feature was directly quantified by the ratio  $\Gamma_{s/l}$ . Image analysis revealed  
501 that these small particles have diameter of around 5 nm (around the resolution limit of the TEM  
502 microscope) to 50 nm (data not shown), which was in agreement with the size range of the

503 population B modelled by SAXS measurements (from 6.1 nm to 21.9 nm in radius – Table 2).  
504 This correlation between the increase in  $n_b$  and  $\Gamma_{s/l}$  suggests that the dense protein regions  
505 detected by SAXS were not only present inside the micelle but could also be present outside the  
506 casein micelle in the diffusible phase, although the composition of the particles outside the  
507 casein micelle is not known.

508 A positive correlation of 0.49 was also observed between  $n_b$  and both NaCl and diffusible Na  
509 (Fig. 2), indicating that NaCl addition increased  $n_b$ . Conversely, enrichment of the suspensions  
510 with  $\text{CaCl}_2$  weakly but significantly, reduced  $n_b$  (correlation coefficient of - 0.39) (Fig. 7). Small  
511 particles of around 20 nm in diameter were also observed by Müller-Buschbaum, Gebhardt,  
512 Roth, Metwalli, & Doster (2007) using atomic force microscopy under similar conditions. These  
513 authors reported a decrease of the number of small particles in the presence of increasing Ca,  
514 consistent with observations here. To date, only the present study and that of Müller-Buschbaum  
515 et al., (2007) report the presence of dissociated aggregates outside of the casein micelle based  
516 on observations by microscopy and SAXS. It is reasonable to assume, however, that such small  
517 particles would not sediment by ultracentrifugation and a parallel can be established between  
518 our observations and the increasing presence of caseins in the supernatant obtained by  
519 ultracentrifugation, defined as soluble caseins. Our observations are also consistent with  
520 Famelart et al., (1999); Zhao & Corredig, (2015), who reported an increase in the concentration  
521 of soluble casein after NaCl addition. Conversely, Famelart et al., (1999); Philippe et al., (2005);  
522 Udabage et al., (2000) observed a decrease in soluble caseins when  $\text{CaCl}_2$  was added. This  
523 may be explained by considering the actions of these two ions. NaCl would be responsible for  
524 the disruption and loosening of the internal structure of the casein micelle by neutralizing  
525 negative charges on the casein chains, whereas  $\text{CaCl}_2$  would either favor the creation of new  
526 bonds between the phosphorylated caseins and/or prevent the dissociation of casein materials  
527 by limiting the solubilization of CaP nanoclusters. Our finding of an increase in soluble casein

528 due to pH-induced dissociation of CaP nanoclusters is also consistent with reports by Dalgleish  
529 & Law, (1989); Le Graet & Gaucheron, (1999); and van Hooydonk et al., (1986).

530  
531 In the present study, there was no significant correlation between pH and  $n_b$  (Fig. 2). There was  
532 however, a direct and strong effect of pH on  $n_{cCaP}$  (the number of population C scatterers per  
533 micelle, correlation of 0.81), which correlates negatively with  $n_b$  (- 0.45) (Fig. 2).  $CaCl_2$  addition  
534 had no significant impact on the size of the dense regions (Fig. 7), while NaCl caused their  
535 decrease, as shown by the correlation between  $r_b$ , and the concentration of NaCl and therefore  
536 diffusible Na and Cl (- 0.50, - 0.53 and - 0.45, respectively) (Fig. 2). The decrease of population  
537 C also led to a decrease in size of the dense regions (correlation coefficient of 0.47 between  
538  $n_{cCaP}$  and  $r_b$ ) (Fig. 2). Finally, it is interesting to note that  $n_b$  and  $r_b$  were inversely correlated (-  
539 0.59) (Fig. 2), meaning that the more dense the regions within the micelle, the smaller the size of  
540 these regions.

### 541 **3.1.2.3 Population C: CaP nanoclusters or protein inhomogeneities**

542 The mean radius of population C ( $r_c$ ) ranged from 1.5 to 1.7 nm, for the set of suspensions  
543 studied with a RSD of 3.1 % (Table 2). This indicates that this population is of similar size in  
544 each suspension, regardless of the physico-chemical modifications applied. However, the  
545 number per casein micelle,  $n_{cCaP}$ , varied from 75 to 244. Considering this population as CaP, the  
546 number is close, although lower than the values of CaP nanoclusters in a native casein micelle  
547 which has been calculated as ~285 by de Kruif, Huppertz, Urban & Petukhov, (2012). In our  
548 experiments, the suspension of NPC powder in water caused ~20 % of the colloidal CaP to  
549 dissolve (calculated based on the colloidal and diffusible contents of the CTRL sample) (Table  
550 1). This reduction in CaP could explain the discrepancy with the data of de Kruif and colleagues.  
551 The number observed, however, is consistent with the findings of Bouchoux et al., (2010), who  
552 reported ~210 CaP nanoclusters per casein micelle.

553 If the population C scatterers were considered as protein inhomogeneities, their number per  
554 casein micelle varied from 140 to 453, which is about 17 times lower than the value found by  
555 Ingham et al., (2016) (Table 2). This difference may be due to the application of a simple sphere  
556 form factor in this study compared to the combination of a Sorensen form factor and hard sphere  
557 structure factor used by Ingham et al., (2016). Our approach was nevertheless sufficient to fit the  
558 SAXS pattern in the high q-region (Fig. 5). The properties of the C-scatterers *i.e.* constant size  
559 and varying number of C-scatterers per casein micelle indicated the disappearance of this  
560 population adhered to an “all-or-nothing” rule, where population C either “dissolved” completely  
561 upon modification of the environment or remained intact within the casein micelle.

562 According to the PCA analysis,  $n_{\text{CaP}}$  correlated highly with pH (0.80), concentrations of colloidal  
563 Ca and Pi (0.86 and 0.80, respectively) and with concentration of diffusible Pi (- 0.84) (Fig. 2),  
564 indicating that the high q feature disappeared with the pH-induced dissolution of colloidal CaP.  
565 Similar pH induced changes in SAXS patterns of casein micelles were reported by Ingham et al.,  
566 (2016) and Marchin et al., (2007). The disappearance of the high q feature was also observed  
567 when colloidal CaP was removed from the casein micelle by the use of chelating agents (EDTA  
568 or  $\text{Na}_3\text{Cit}$ ) (Day et al., 2017; Ingham et al., 2016; Marchin et al., 2007; Pitkowski, Nicolai, &  
569 Durand, 2007). These correlations are therefore consistent with the assignment of this  
570 population as CaP nanoclusters, as suggested by Holt, de Kruif, Tuinier, & Timmins, (2003).  
571 The correlations between  $n_{\text{CaP}}$  noted above are not inconsistent, however, with the hypothesis  
572 of Ingham et al. (2016) *i.e.* that this population of particles corresponds to protein  
573 inhomogeneities. In this case, protein inhomogeneities would be closely linked to micellar CaP.  
574 Dissolution of the CaP from the casein micelle would also induce the disruption of the protein  
575 inhomogeneities. Such an arrangement would be in agreement with the dual binding model of  
576 Horne, (1998), that considers CaP nanoclusters not only as crosslinking agents but also as  
577 charge neutralizers between casein chains that allow proteins to form more hydrophobic  
578 interactions. Further analysis in the form of cross comparisons between the evolution of the high

579  $q$  SAXS shoulder and the specific intensity variation at  $q = 0.035 \text{ \AA}^{-1}$  observed either in SANS or  
580 resonant X-ray scattering would bring interesting information about this CaP nanocluster /  
581 protein inhomogeneity dependency. Finally,  $n_{\text{CaP}}$  correlated negatively with  $n_b$  (- 0.45) and with  
582  $\Gamma_{s/l}$  (-0.43), and correlated positively with  $r_b$  (0.47) (Fig. 2). Whilst these correlations could arise  
583 from a number of structural changes within the micelle, they suggest that protein from the  
584 micelle is being released into the diffusible phase.

### 585 **3.2 Coagulation properties of the modified casein micelles**

586 The RCT and the maximum firmness of the gel, defined here as firmness, were determined for  
587 the 27 suspensions using data obtained from the firmness curves (Fig. 8). These two  
588 parameters were linked to the other colloidal and structural variables through PCA and multiple  
589 linear regression analyses.

#### 590 **3.2.1 Rennet clotting time**

591 The use of rennet made the 27 suspensions clot between 1.1 to 42.4 min (RSD of 113.5%)  
592 (Table 3). This large variability was first ascribed to the variation in pH, as there was a significant  
593 correlation between RCT and pH with a coefficient of 0.69 (Fig. 2). A consequence of the pH  
594 decrease was the solubilization of the micellar Ca and Pi (section 3.1.1). Therefore RCT also  
595 positively correlated with the concentration of colloidal Ca and Pi, and with diffusible Pi with  
596 coefficients of 0.49, 0.61 and - 0.61, respectively (Fig. 2). A reduction in RCT as a result of a  
597 decrease in pH has been well described in the literature (Choi et al., 2007; Daviau et al., 2000;  
598 Karlsson et al., 2007; Zoon et al., 1989). This has been ascribed to the enhancement of enzyme  
599 activity and a decrease in the electrostatic repulsion between paracaseinates at low pH that  
600 favored aggregation.

601 A weaker but significant and positive correlation was also observed between diffusible Na and  
602 RCT (0.39) (Fig. 2), meaning that an increased concentration of this ion in the diffusible phase  
603 led to an increase in the RCT. Similar effects of added NaCl have been also reported by (Bulca  
604 et al., 2016; Famelart et al., 1999; Grufferty & Fox, 1985; Karlsson et al., 2007; Sbodio et al.,

605 2006; Zhao & Corredig, 2015; Zoon et al., 1989) and were attributed to a decrease in the rate of  
606 the rennet enzyme due to the screening of charges on  $\kappa$ -casein and the enzyme.

607  
608 The negative correlations of RCT with  $\tau$  and  $r_a$  (- 0.47 and - 0.53, respectively) (Fig. 2) indicated  
609 that large micelles clotted more quickly than small ones, a finding that was opposite to those  
610 made in the studies of Ekstrand, (1980) and Ford & Grandison, (1986). The increase of the  
611 micellar size in the present study was a consequence of the pH decrease that caused the  
612 micelles to swell and also potentially caused other structural changes. The correlation between  
613 these two factors is probably a disguised effect of the pH and the effect of pH on both micelle  
614 size and structure. In the two previous studies with opposing findings, the micelles were  
615 fractionated according to their size by ultracentrifugation and did not undergo any physico-  
616 chemical treatment, which could further explain these differences.

### 617 **3.2.2 Firmness of the rennet gel formed within the first 60 min of coagulation**

618 Although the firmness was highly variable, with an RSD of 34 % (Table 3) within the set of  
619 suspensions, this variable did not correlate directly with the other colloidal and structural  
620 characteristics of the casein micelle suspensions. Indeed, the firmness, concentrations of  $\text{CaCl}_2$   
621 and concentrations of diffusible Ca were the only well-projected variables as defined by the 3<sup>rd</sup>  
622 and 4<sup>th</sup> dimensions of the PCA analysis (Fig. 4). Vectors representing concentrations of  $\text{CaCl}_2$   
623 and diffusible Ca were orthogonal to the vector for firmness, reflecting no correlations between  
624 these variables. However, PCA estimates the first order correlations between variables, and  
625 does not take into account the interactions that might exist between the different features.

626 A second statistical approach, multiple linear regression, was therefore used to assess the effect  
627 of possible interactions between variables on the firmness of the rennet gels. Structural SAXS  
628 features revealed to be excellent candidates for this complementary analysis for two reasons.  
629 Firstly, these variables were unique and interesting descriptors reporting information at three  
630 different structural levels: 1) the casein micelle, 40 to 60 nm in radius and previously described

631 as population A; 2) the dense regions, 6 to 22 nm in radius and previously described as  
632 population B; 3) the CaP nanoclusters (or protein inhomogeneities), 1.5 to 1.7 nm in radius and  
633 previously described as population C. Secondly, these variables correlated significantly with the  
634 whole set of colloidal and mineral features determined by other techniques and constituted a  
635 way to summarize the whole set of data. Therefore,  $r_a$ ,  $n_b$  and  $n_{cCaP}$  were subject to linear  
636 regression in order to define a predictive model of the firmness that considered the quadratic  
637 effects and the second order interactions between these variables. For consistency, the values  
638 of  $n_{cCaP}$  used in this statistical analysis were determined considering population C as CaP  
639 nanoclusters. This would make no difference in the properties of the model, as there was a  
640 proportional relationship linking  $n_{cCaP}$  for CaP nanoclusters and  $n_{cPI}$  for protein inhomogeneities.  
641 Based on the experimental design, the following model equation was established to predict the  
642 maximum firmness of the rennet gels made from the suspensions:

$$643 \text{ Firmness} = 187.3 - 3.5 \times r_a - 1.2 \times n_b - 0.9 \times n_{cCaP} + 0.02 \times (r_a \times n_c) \quad (9)$$

644 where  $r_a$  was the radius of the casein micelle,  $n_b$  and  $n_{cCaP}$  were the number of dense regions  
645 and CaP nanoclusters per casein micelle, respectively. This model explained 68.5% of the  
646 variability of the firmness. Statistical analysis also revealed that the interaction between  $r_a$  and  $n_c$   
647 ( $r_a \times n_c$ ) and the first order effect of  $n_b$  in this model were significant. These two contributions had  
648 a statistical weight of 35.3% and 27 % in the model, respectively.

649 Figure 9.A and B. displays each suspension in the first four dimensions of the PCA. The  
650 suspensions are colored according to their firmness (orange for weak, red for medium, black for  
651 strong). Figure 9.A represents the evolution of firmness within the set of samples, defined by  
652 PCs 3 and 4 with the arrow pointing in the direction of increasing firmness (the same direction as  
653 seen in Figure 4). The negative coefficient assigned to  $n_b$  in the firmness equation model  
654 indicates that the release of protein from the casein micelles led to the formation of weaker gels.  
655 This direct effect is well illustrated when reading Figure 9.A from the bottom right corner

656 (suspension G, U - poor in dense regions and stronger gels) to the upper left corner (suspension  
657 B - rich in dense regions and a weaker gel).

658 As described earlier, the release of dense regions was favored by the addition of NaCl and  
659 limited by the addition of CaCl<sub>2</sub>. The influence of NaCl on the firmness has been examined by  
660 several groups but conflicting results have been reported. Consistent with the results reported  
661 here, Famelart et al., (1999) and Grufferty & Fox (1985) did not observe any modification of the  
662 moduli or the curd tension of the rennet gels upon addition of NaCl. However, Bulca et al.,  
663 (2016) and Zhao & Corredig, (2015) reported a decrease in the firmness or stiffness of the  
664 rennet gels. While Zoon et al., (1989) observed higher moduli for 8h aged gels supplemented in  
665 NaCl but lower moduli was observed only 1 h after the addition of rennet to the milk,  
666 corresponding to the experimental conditions of the present study. The negative effect of NaCl  
667 on the firmness of rennet gels is poorly explained in the literature. A competition between Na<sup>+</sup>  
668 and Ca<sup>2+</sup> has been proposed, as well as the screening of casein charges and in some cases, the  
669 solubilization of the micellar CaP (Grufferty & Fox, 1985; Zhao & Corredig, 2015). Based on the  
670 significant correlations that link  $n_b$  and NaCl and the significant negative effect of  $n_b$  on the  
671 firmness of the rennet gel, we would argue that the decrease in firmness observed with the  
672 addition of NaCl is due to the release of protein from the casein micelles. This explanation is  
673 similar to that of Gaygadzhiev, Massel, Alexander, & Corredig, (2012), who found that the  
674 addition of sodium caseinate to milk inhibited the aggregation of casein micelles. In this case,  
675 the soluble dense regions may adsorb on the surface of the paracaseinate formed after rennet  
676 addition, causing an increase in the steric repulsion between the rennet-altered particles which  
677 would limit the aggregation phenomenon and the formation of a firm network.

678 In contrast, there is a general consensus that CaCl<sub>2</sub> addition increases gel firmness (Deeth &  
679 Lewis, 2015; Sandra et al., 2012; Zoon et al., 1988). In this case, this improvement was  
680 attributed to the ability of Ca to preserve the number of CaP bonds between the caseins within  
681 the micelle but also within the casein gel network. It was demonstrated in section 3.1.2.2, that

682 CaCl<sub>2</sub> addition limited the release of dense regions, which consequently had a positive impact  
683 on the firmness of the gels through the decrease of  $n_b$ .

684

685 The effect of the interaction between  $r_a$  and  $n_{cCaP}$  appears to be more subtle. The direct effect of  
686  $r_a$  could be seen in figure 9.B from the upper right corner (suspension M - small casein micelle)  
687 to the bottom left corner (suspension A, D, O - large and swollen casein micelle). There were no  
688 direct and simple consequences of  $r_a$  on the gel firmness. This can be illustrated by the medium  
689 size micelles (center of the graph, suspensions B, S, V, L for instance) that can either form  
690 weak, medium or strong gels. This result was quite consistent with the observation of Dalgleish,  
691 Brinkhuis, & Payens, (1981) who found no dependence between the size of micelles and their  
692 coagulation. Yet, several authors have reported that small casein micelles form stronger gels  
693 (Ford & Grandison, 1986; Logan et al., 2015; Niki, Kohyama, Sano, & Nishinari, 1994). However,  
694 in these studies, the micelles were in their native state because they were either isolated from  
695 milk by ultracentrifugation or were in milk samples that were selected from cows who produced  
696 small casein micelles. In contrast, the present study involved modifications to the environment  
697 that affected the size of the casein micelles.

698 The direct effect of  $n_{cCaP}$  can be observed in figure 9.B from the upper left corner (suspension B  
699 – poor in population C) to the bottom right corner (suspensions L, Y – rich in population C) but  
700 no direct dependency of gel firmness on  $n_{cCaP}$  was observed. This population may be either CaP  
701 nanoclusters or protein inhomogeneities. In both cases, the presence of such interactions,  
702 whether they are mineral-protein or protein-protein interactions, would create more crosslinking  
703 points resulting in a stronger gel network.

704 The literature reports a quadratic relationships between pH and rennet gel firmness, *i.e.* there is  
705 a parabolic increase in the gel firmness with pH up to a maximum value, followed by a parabolic  
706 decrease in firmness (Choi et al., 2007; Karlsson et al., 2007; Lucey, Johnson, & Horne, 2003;  
707 Zoon et al., 1989). A change in pH modifies the ionization of individual amino acids, either

708 increasing or decreasing the electrostatic interactions between casein chains. A simultaneous  
709 consequence is the solubilization of the micellar CaP at lower pH, which decreases the attractive  
710 interactions between casein molecules. The addition of a chelating agent to milk or casein  
711 suspension similarly leads to the solubilization of micellar CaP (de Kort et al., 2011; McCarthy et  
712 al., 2017; Mizuno & Lucey, 2005; Pitkowski et al., 2007) and causes a decrease in the firmness  
713 of the rennet gels (Choi et al., 2007).

714 At this point, it is important to remember that the variations of  $r_a$  and  $n_{cCaP}$  were not impacted by  
715 only one factor (size fractionation, or pH, or chelating agent addition) but by the simultaneous  
716 effect of three factors (pH, NaCl and CaCl<sub>2</sub>). Therefore, the firmness modeling reveals that the  
717 interaction between those variables should be considered. The interaction between  $r_a$  and  $n_{cCaP}$   
718 on the rennet gel firmness means that the firmness at a given  $r_a$  depended on  $n_{cCaP}$  and vice  
719 versa. As an example to illustrate this interaction, suspensions containing medium sized casein  
720 micelles (from 45 to 47 nm in radius) can lead to the formation of weaker gels if the amount of C-  
721 particles is too low (suspension B). Yet these micelles formed medium strength gels  
722 (suspensions P, E, C) if their C-particle content increased, or even stronger gels when those  
723 casein micelles are rich in C-particles (suspensions X, I, T). Similarly, small casein micelles that  
724 were rich in C-particles formed weaker gels (suspension W, K, M) but an increase in micelle size  
725 led to an increase in gel firmness (suspension H, V, T). Large casein micelles, depleted in C  
726 particles (suspension A, O, D) also formed weaker gels.

727

#### 728 **4 Conclusion**

729 The multifactorial experimental design applied here allowed the effect of three variables: pH,  
730 NaCl and CaCl<sub>2</sub> on the colloidal and rennet coagulation properties of casein micelles to be  
731 assessed and ranked. Variations in pH had the strongest influence on the mineral balance of the  
732 casein micelles. A decrease in pH caused the colloidal CaP to solubilize. In contrast, NaCl  
733 addition had no impact on the mineral content of the casein micelle. The solubilization of

734 colloidal CaP caused the micelle to shrink while the addition of NaCl reduced the size of the  
735 casein micelle due to the release of small particles into the diffusible phase. The presence of  
736 such particles, around 25 nm in diameter, was strongly supported by experimental SAXS data  
737 combined with observations by cryo-TEM. These particles are believed to be part of the dense  
738 regions described by Bouchoux et al. (2010); here they were observed both inside and outside  
739 of the casein micelle. CaCl<sub>2</sub> had no effect on the casein micelle size but prevented disruption of  
740 the dense regions within the micelle. The SAXS data also revealed the presence of a high-q  
741 structural feature (the C-population), that were of a constant size (~1.6 nm in radius) but varied  
742 in number with different environmental conditions. Their presence was strongly dependent to the  
743 CaP content of the casein micelle. This feature could be assigned to the presence of either CaP  
744 nanoclusters or protein inhomogeneities.

745 The renneting properties were most impacted by a decrease in pH, causing a reduction in RCT,  
746 while NaCl supplementation led to longer RCT. Variations in gel firmness were more complex  
747 but could be explained by considering the interactions between the size of the casein micelle,  
748 the C-population and the dissociation of dense regions within the casein micelle.

749 Together the data presented here illustrate the complex interactions of three variables on the  
750 properties of casein micelles in a simple model system relevant to products such as purified  
751 casein micelles, fractionated from milk and prepared by diafiltration. This study provides a  
752 framework that links existing literature on the effect of single variables and improves our  
753 understanding of how the properties of casein micelles can be manipulated to control micelle  
754 size, structure and functional properties. It also provides a basis for future studies to examine  
755 casein micelles in more complex dairy product matrices and as a function of processing.

756

## 757 **5 Acknowledgment**

758 Acknowledgements are given to François Boué for the interesting discussions regarding the  
759 modeling of the SAXS data, to Arlette Leduc for assistance in the analysis of the minerals, to Mi

760 Xu for assistance with data collection at the Australian Synchrotron and the Biological Optical  
761 Microscopy Platform (BOMP) at the Bio21 Molecular Science and Biotechnology Institute for  
762 access to equipment.

763 Fundings: This work was supported by the French Dairy Interbranch Organization (CNIEL) for  
764 their financial support and by Chr Hansen through the loan of a Chymograph®. Sally Gras and  
765 Lydia Ong are supported by the Australian Research Council's Industrial Transformation  
766 Research Program (ITRP) funding scheme (project number IH120100005). The ARC Dairy  
767 Innovation Hub is a collaboration between the University of Melbourne, The University of  
768 Queensland and Dairy Innovation Australia Ltd. The SAXS experiments were undertaken on the  
769 SAXS/WAXS beamline at the Australian Synchrotron, Victoria, Australia (Proposal No.  
770 AS163/SAXS/11019).

771

## 772 **6 References**

- 773 Abdi, H., & Williams, L. J. (2010). Principal component analysis. *Wiley Interdisciplinary Reviews:*  
774 *Computational Statistics*, 2(4), 433–459.
- 775 Aoki, T., Umeda, T., & Nakao, T. (1999). Effect of sodium chloride on the properties of casein  
776 micelles, *Milchwissenschaft*, 54(2), 91–93.
- 777 Bouchoux, A., Gésan-Guiziou, G., Pérez, J., & Cabane, B. (2010). How to squeeze a sponge:  
778 casein micelles under osmotic stress, a SAXS study. *Biophysical Journal*, 99(11), 3754–3762.
- 779 Bouchoux, A., Ventureira, J., Gésan-Guiziou, G., Garnier-Lambrouin, F., Qu, P., Pasquier, C.,  
780 Pézenec, S., Schweins, R., Cabane, B. (2015). Structural heterogeneity of milk casein micelles:  
781 a SANS contrast variation study. *Soft Matter*, 11(2), 389–399.
- 782 Broyard, C., & Gaucheron, F. (2015). Modifications of structures and functions of caseins: a  
783 scientific and technological challenge. *Dairy Science & Technology*, 95(6), 831-862

784 Bulca, S., Wolfschoon-Pombo, A., & Kulozik, U. (2016). Rennet coagulation properties of UHT-  
785 treated phosphocasein dispersions as a function of casein and NaCl concentrations.  
786 *International Journal of Dairy Technology*, 69(3), 328–336.

787 Chen, Y.-Y., Peng, B., Yang, Q., Glew, M. D., Veith, P. D., Cross, K. J., Goldie, K.N., Chen, D.,  
788 O'Brien-Simpson, N., Dashper, S.G., Reynolds, E. C. (2011). The outer membrane protein LptO  
789 is essential for the O-deacylation of LPS and the co-ordinated secretion and attachment of A-  
790 LPS and CTD proteins in *Porphyromonas gingivalis*: LptO-dependent maturation of A-LPS and  
791 CTD proteins. *Molecular Microbiology*, 79(5), 1380–1401.

792 Choi, J., Horne, D. S., & Lucey, J. A. (2007). Effect of insoluble calcium concentration on rennet  
793 coagulation properties of milk. *Journal of Dairy Science*, 90(6), 2612–2623.

794 Dalgleish, D. G., Brinkhuis, J., & Payens, T. A. J. (1981). The coagulation of differently sized  
795 casein micelles by rennet. *European Journal of Biochemistry*, 119(2), 257–261.

796 Dalgleish, D. G., & Corredig, M. (2012). The Structure of the Casein Micelle of Milk and Its  
797 Changes During Processing. *Annual Review of Food Science and Technology*, 3(1), 449–467.

798 Dalgleish, D. G., & Law, A. J. R. (1989). pH-Induced dissociation of bovine casein micelles. II.  
799 Mineral solubilization and its relation to casein release. *Journal of Dairy Research*, 56(05), 727.

800 Daviau, C., Famelart, M.-H., Pierre, A., Gouedranche, H., & Maubois, J.-L. (2000). Rennet  
801 coagulation of skim milk and curd drainage: effect of pH, casein concentration, ionic strength  
802 and heat treatment. *Le Lait*, 80(4), 397–415.

803 Day, L., Raynes, J. K., Leis, A., Liu, L. H., & Williams, R. P. W. (2017). Probing the internal and  
804 external micelle structures of differently sized casein micelles from individual cows milk by  
805 dynamic light and small-angle X-ray scattering. *Food Hydrocolloids*, 69, 150–163.

806 de Kort, E., Minor, M., Snoeren, T., van Hooijdonk, T., & van der Linden, E. (2011). Effect of  
807 calcium chelators on physical changes in casein micelles in concentrated micellar casein  
808 solutions. *International Dairy Journal*, 21(12), 907–913.

809 de Kruif, C. G. (1999). Casein micelle interactions. *International Dairy Journal*, 9(3–6), 183–188.

810 de Kruif, C. G. (2014). The structure of casein micelles: a review of small-angle scattering data.  
811 *Journal of Applied Crystallography*, 47(5), 1479–1489.

812 de Kruif, C. G., & Zhulina, E. B. (1996). k-casein as a polyelectrolyte brush on the surface of  
813 casein micelles. *Colloids and Surfaces A: Physicochemical and Engineering Aspects*, 117(1–2),  
814 151–159.

815 Deeth, H. C., & Lewis, M. J. (2015). Practical consequences of calcium addition to and removal  
816 from milk and milk products. *International Journal of Dairy Technology*, 68(1), 1–10.

817 Ekstrand, B., Larsson-Raznikiewicz, M., Perlmann, C. (1980). Casein micelle size and  
818 composition related to the enzymatic coagulation process. *Biochimica et Biophysica Acta-  
819 General Subjects*, 630(3), 361–366.

820 Famelart, M.-H., Le Graet, Y., & Raulot, K. (1999). Casein micelle dispersions into water, NaCl  
821 and CaCl<sub>2</sub>: physicochemical characteristics of micelles and rennet coagulation. *International  
822 Dairy Journal*, 9, 293–297.

823 Famelart, M.-H., Lepasant, F., Gaucheron, F., Le Graet, Y., & Schuck, P. (1996). pH-Induced  
824 physicochemical modifications of native phosphocaseinate suspensions: Influence of aqueous  
825 phase. *Le Lait*, 76(5), 445–460.

826 Ford, G. D., & Grandison, A. S. (1986). Effect of size of casein micelles on coagulation  
827 properties of skim milk. *Journal of Dairy Research*, 53(01), 129.

828 Gaucheron, F. (2004). *Minéraux et produits laitiers*. Paris: Technique & Documentation.

829 Gaygadzhiev, Z., Massel, V., Alexander, M., & Corredig, M. (2012). Addition of sodium caseinate  
830 to skim milk inhibits rennet-induced aggregation of casein micelles. *Food Hydrocolloids*, 26(2),  
831 405–411.

832 Grufferty, M. B., & Fox, P. F. (1985). Effect of added NaCl on some physicochemical properties  
833 of milk, *Irish Journal of Food Science and Technology*, 9(1), 1–9.

834 Guinee, T. P., Gorry, C. B., O'Callaghan, D. J., O'Kennedy, B. T., O'Brie, N., Fenelon, M. A.  
835 (1997). The effects of composition and some processing treatments on the rennet coagulation  
836 properties of milk. *International Journal of Dairy Technology*. 50(3), 99-106

837 Holt, C., Carver, J. A., Ecroyd, H., & Thorn, D. C. (2013). Invited review: Caseins and the casein  
838 micelle: Their biological functions, structures, and behavior in foods. *Journal of Dairy Science*,  
839 96(10), 6127–6146.

840 Holt, C, de Kruif, C. G., Tuinier, R., & Timmins, P. A. (2003). Substructure of bovine casein  
841 micelles by small-angle X-ray and neutron scattering. *Colloids and Surfaces A: Physicochemical  
842 and Engineering Aspects*, 213(2–3), 275–284.

843 Holt, C., Timmins, P. A., Errington, N., & Leaver, J. (1998). A core-shell model of calcium  
844 phosphate nanoclusters stabilized by beta-casein phosphopeptides, derived from sedimentation  
845 equilibrium and small-angle X-ray and neutron-scattering measurements. *European Journal of  
846 Biochemistry*, 252(1), 73–78.

847 Holt, C. (2016). Casein and casein micelle structures, functions and diversity in 20 species.  
848 *International Dairy Journal*, 60, 2–13.

849 Holt, C., & Horne, D. S. (1996). The hairy casein micelle : Evolution of the concept and its  
850 implications for dairy technology. *Nederlands Melk En Zuiveltijdschrift*, 50(2), 85–111.

851 Horne, D. S. (1998). Casein interactions: casting light on the black boxes, the structure in dairy  
852 products. *International Dairy Journal*, 8(3), 171–177.

853 Horne, D. S. (2017). A balanced view of casein interactions. *Current Opinion in Colloid &  
854 Interface Science*, 28, 74–86.

855 Ingham, B., Erlangga, G. D., Smialowska, A., Kirby, N. M., Wang, C., Matia-Merino, L.,  
856 Haverkamp, R.G., Carr, A. J. (2015). Solving the mystery of the internal structure of casein  
857 micelles. *Soft Matter*, 11(14), 2723–2725.

858 International Dairy Federation. (2014). Milk and milk products - Determination of nitrogen content  
859 - Part 1: Kjeldahl principle and crude protein calculation.

860 Ingham, B., Smialowska, A., Erlangga, G. D., Matia-Merino, L., Kirby, N. M., Wang, C.,  
861 Haverkamp, R. G., Carr, A. J. (2016). Revisiting the interpretation of casein micelle SAXS data.  
862 *Soft Matter*, 12(33), 6937–6953.

863 Jolliffe I. (2011) *Principal Component Analysis*. Berlin: Springer

864 Karlsson, A. O., Ipsen, R., & Ardö, Y. (2007). Influence of pH and NaCl on rheological properties  
865 of rennet-induced casein gels made from UF concentrated skim milk. *International Dairy Journal*,  
866 17(9), 1053–1062.

867 Karlsson, A. O., Ipsen, R., Schrader, K., & Ardö, Y. (2005). Relationship between physical  
868 properties of casein micelles and rheology of skim milk concentrate. *Journal of Dairy Science*,  
869 88(11), 3784–3797.

870 Lazzaro, F., Saint-Jalmes, A., Violleau, F., Lopez, C., Gaucher-Delmas, M., Madec, M.-N.,  
871 Beaucher, E., Gaucheron, F. (2017). Gradual disaggregation of the casein micelle improves its  
872 emulsifying capacity and decreases the stability of dairy emulsions. *Food Hydrocolloids*, 63,  
873 189–200.

874 Le Graet, Y., & Brulé, G. (1993). Les équilibres minéraux du lait : influence du pH et de la force  
875 ionique, *Le Lait*, 73(1), 51–60.

876 Le Graet, Y., & Gaucheron, F. (1999). pH-induced solubilization of minerals from casein  
877 micelles: influence of casein concentration and ionic strength, *Journal of Dairy Research*, 66(2),  
878 215–224.

879 Le Ray, C., Maubois, J.-L., Gaucheron, F., Brulé, G., Pronnier, P., & Garnier, F. (1998). Heat  
880 stability of reconstituted casein micelle dispersions: changes induced by salt addition. *Le Lait*,  
881 78(4), 375–390.

882 Lê, S., Josse, J., & Husson, F. (2008). FactoMineR: An R package for multivariate analysis.  
883 *Journal of Statistical Software*, 25(1).

884 Logan, A., Leis, A., Day, L., Øiseth, S. K., Puvanenthiran, A., & Augustin, M. A. (2015). Rennet  
885 gelation properties of milk: Influence of natural variation in milk fat globule size and casein  
886 micelle size. *International Dairy Journal*, *46*, 71–77.

887 Lucey, J. A. (2002). Formation and physical properties of milk protein gels. *Journal of Dairy*  
888 *Science*, *85*(2), 281–294.

889 Lucey, J. A., Johnson, M. E., & Horne, D. S. (2003). Invited review: Perspectives on the basis of  
890 the rheology and texture properties of cheese. *Journal of Dairy Science*, *86*(9), 2725–2743.

891 Marchin, S., Putaux, J.-L., Pignon, F., & Léonil, J. (2007). Effects of the environmental factors on  
892 the casein micelle structure studied by cryo transmission electron microscopy and small-angle x-  
893 ray scattering/ultrasmall-angle x-ray scattering. *The Journal of Chemical Physics*, *126*(4),  
894 045101.

895 McCarthy, N. A., Power, O., Wijayanti, H. B., Kelly, P. M., Mao, L., & Fenelon, M. A. (2017).  
896 Effects of calcium chelating agents on the solubility of milk protein concentrate. *International*  
897 *Journal of Dairy Technology*, *70*(3), 415–423.

898 Mishra, R. I., Govindasamy-Lucey, S. E., Lucey, J. A. (2005). Rheological properties of rennet-  
899 induced gels during the coagulation and cutting process: impact of processing conditions.  
900 *Journal of texture studies*. *36*(2), 190-212.

901 Mizuno, R., & Lucey, J. A. (2005). Effects of emulsifying salts on the turbidity and calcium-  
902 phosphate–protein interactions in casein micelles. *Journal of Dairy Science*, *88*(9), 3070–3078.

903 Moitzi, C., Menzel, A., Schurtenberger, P., & Stradner, A. (2011). The pH induced Sol–Gel  
904 transition in skim milk revisited. A detailed study using time-resolved light and X-ray scattering  
905 experiments. *Langmuir*, *27*(6), 2195–2203.

906 Müller-Buschbaum, P., Gebhardt, R., Roth, S. V., Metwalli, E., & Doster, W. (2007). Effect of  
907 calcium concentration on the structure of casein micelles in thin films. *Biophysical Journal*, *93*(3),  
908 960–968.

909 Niki, R., Kohyama, K., Sano, Y., & Nishinari, K. (1994). Rheological study on the rennet-induced  
910 gelation of casein micelles with different sizes. *Polymer Gels and Networks*, 2(2), 105–118.

911 Ouanezar, M., Guyomarc'h, F., & Bouchoux, A. (2012). AFM imaging of milk casein micelles:  
912 Evidence for structural rearrangement upon acidification. *Langmuir*, 28(11), 4915–4919.

913 Philippe, M, Le Graet, Y., & Gaucheron, F. (2005). The effects of different cations on the  
914 physicochemical characteristics of casein micelles. *Food Chemistry*, 90(4), 673–683.

915 Philippe, Marine, Gaucheron, F., Le Graet, Y., Michel, F., & Garem, A. (2003). Physicochemical  
916 characterization of calcium-supplemented skim milk. *Le Lait*, 83(1), 45–59.

917 Pierre, A., Fauquant, J., Le Graet, Y., & Maubois, J.-L. (1992). Préparation de phosphocaseinate  
918 natif par microfiltration sur membrane. *Le Lait*, 72 (5), 461–474.

919 Pignon, F., Belina, G., Narayanan, T., Paubel, X., Magnin, A., & Gésan-Guiziou, G. (2004).  
920 Structure and rheological behavior of casein micelle suspensions during ultrafiltration process.  
921 *The Journal of Chemical Physics*, 121(16), 8138-8146.

922 Pitkowski, A., Nicolai, T., & Durand, D. (2007). Scattering and turbidity study of the dissociation  
923 of the casein by calcium chelation. *Biomacromolecules*, 9, 369–375.

924 Priyashantha, H., Lundh, Å., Höjer, A., Hetta, M., Johansson, M., and Langton, M. (2019).  
925 Interactive effects of casein micelle size and calcium and citrate content on rennet-induced  
926 coagulation in bovine milk. *Journal of Texture Studies*, 1-12.

927 Sandra, S., Ho, M., Alexander, M., & Corredig, M. (2012). Effect of soluble calcium on the  
928 renneting properties of casein micelles as measured by rheology and diffusing wave  
929 spectroscopy. *Journal of Dairy Science*, 95(1), 75–82.

930 Sbodio, O. A., Tercero, E. J., Coutaz, R., & Revelli, G. R. (2006). Effect of rennet and sodium  
931 chloride concentration on milk coagulation properties. *Ciencia Y Tecnologia Alimentaria*, 5(3),  
932 182–188.

933 Schmidt, D. G. (1982). *Developments in Dairy Chemistry: 1. Proteins* (P. F. Fox). London:  
934 Applied Science Publishers.

935 Schuck, P., Piot, M., Méjean, S., Le Graet, Y., Fauquant, J., Brulé, G., & Maubois, J. L. (1994).  
936 Déshydratation par atomisation de phosphocaséinate natif obtenu par microfiltration sur  
937 membrane. *Le Lait*, 74(5), 375–388.

938 Schuck, P., Dolivet, A., Jeantet, R., (2012). *Analytical Methods for Food and Dairy Powders*.  
939 Oxford: John Wiley & Sons

940 Schulz, G. V. (1935). Highly polymerized compounds. CXXII. The relation between reaction rate  
941 and composition of the reaction product in macropolymerization processes. *Zeitschrift für*  
942 *Physikalische Chemie*, B30, 379–398.

943 Shukla, A., Narayanan, T., & Zanchi, D. (2009). Structure of casein micelles and their  
944 complexation with tannins. *Soft Matter*, 5(15), 2884.

945 Silva, N. N., Piot, M., de Carvalho, A. F., Violleau, F., Fameau, A.-L., & Gaucheron, F. (2013).  
946 pH-induced demineralization of casein micelles modifies their physico-chemical and foaming  
947 properties. *Food Hydrocolloids*, 32(2), 322–330.

948 Thorn, D. C., Meehan, S., Sunde, M., Rekas, A., Gras, S. L., MacPhee, C. E., Dobson, C. M.,  
949 Wilson, M. R., Carver, J. A. (2005). Amyloid fibril formation by bovine milk  $\kappa$ -Casein and its  
950 inhibition by the molecular chaperones  $\alpha$  s - and  $\beta$ -Casein. *Biochemistry*, 44(51), 17027–17036.

951 Tran Le, T., Saveyn, P., Hoa, H. D., & Van der Meeren, P. (2008). Determination of heat-  
952 induced effects on the particle size distribution of casein micelles by dynamic light scattering and  
953 nanoparticle tracking analysis. *International Dairy Journal*, 18(12), 1090–1096.

954 Tuinier, R., & de Kruif, C. G. (2002). Stability of casein micelles in milk. *The Journal of Chemical*  
955 *Physics*, 117(3), 1290–1295.

956 Udabage, P., McKinnon, I. R., & Augustin, M. A. (2000). Mineral and casein equilibria in milk:  
957 effects of added salts and calcium-chelating agents, *Journal of Dairy Research*, 67(3), 361–370.

958 Udabage, P., McKinnon, I. R., Augustin, M. A. (2001). Effects of mineral salts and calcium  
959 chelating agents on the gelation of renneted skim milk. *Journal of Dairy Science*. 84(7), 1569-75.

960 van Hooydonk, A. C. M., Boerrigter, I. J., & Hagedoorn, H. G. (1986). pH-induced physico-  
961 chemical changes of casein micelles in milk and their effect on renneting. 2. Effect of pH on  
962 renneting of milk, *Netherland Milk and Dairy Journal*, 40, 297–313.

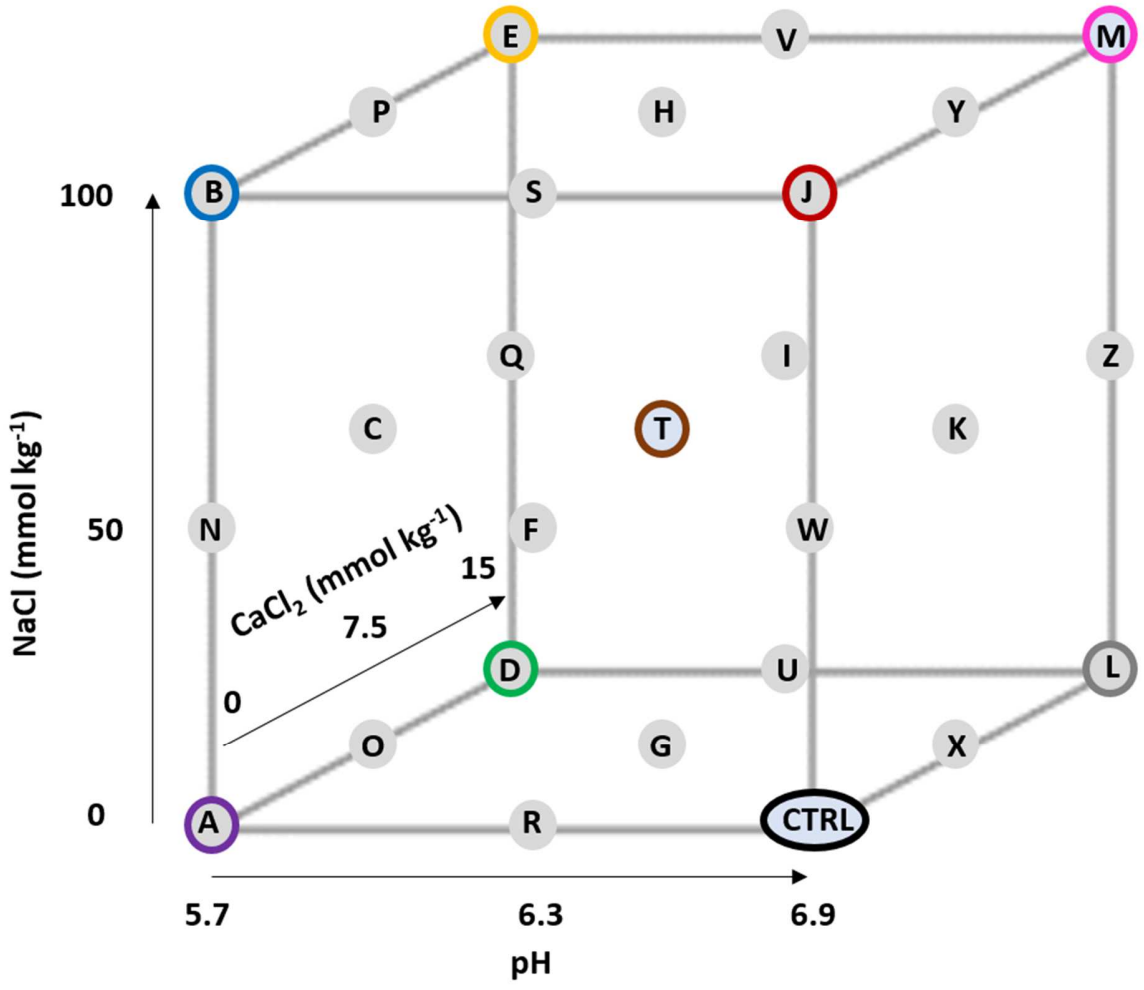
963 Walstra, P. (1999). Casein sub-micelles: do they exist? *International Dairy Journal*, 9(3–6), 189–  
964 192.

965 Wold, S., Esbensen, K., & Geladi, P. (1987). Principal component analysis. *Chemometrics and*  
966 *Intelligent Laboratory Systems*, 2(1–3), 37–52.

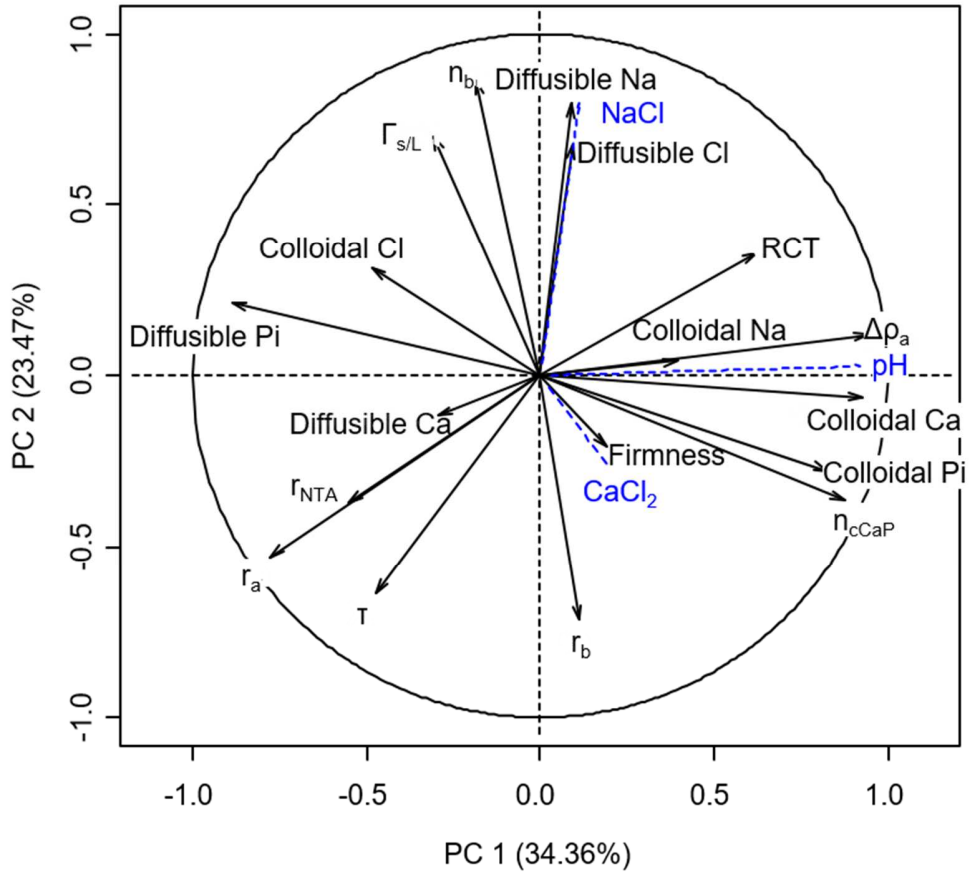
967 Zhao, Z., & Corredig, M. (2015). Changes in the physico-chemical properties of casein micelles  
968 in the presence of sodium chloride in untreated and concentrated milk protein. *Dairy Science &*  
969 *Technology*, 95(1), 87–99.

970 Zoon, P., van Vliet, T., & Walstra, P. (1988). Rheological properties of rennet-induced skim milk  
971 gels. 3. The effect of calcium and phosphate, *Netherland Milk and Dairy Journal*, 42, 295–312.

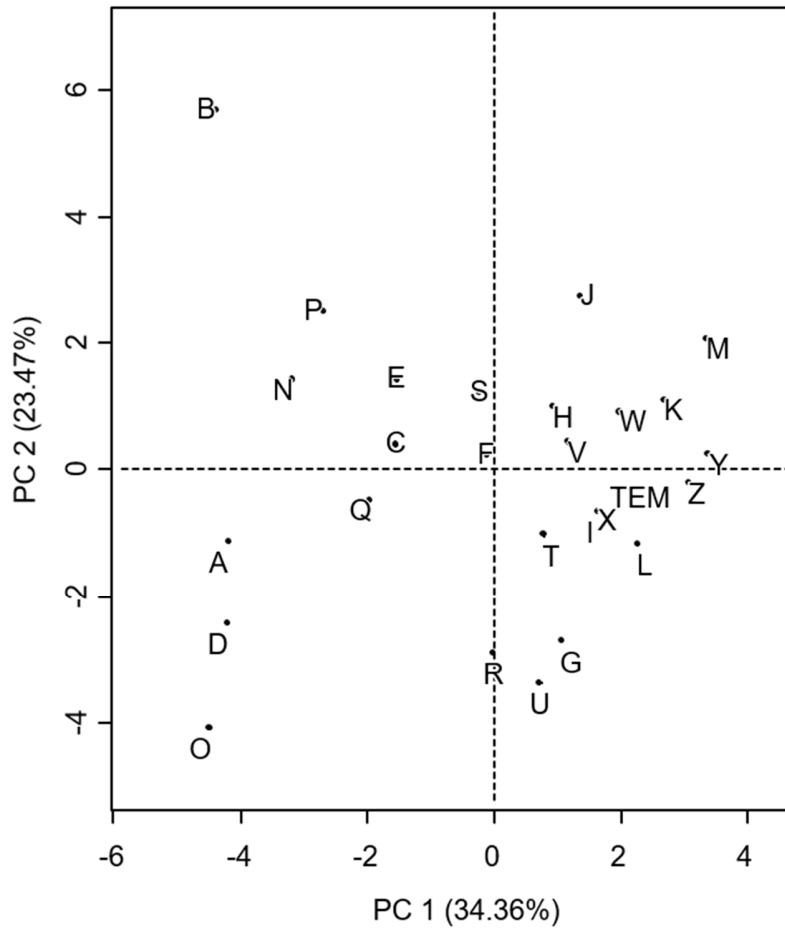
972 Zoon, P., van Vliet, T., & Walstra, P. (1989). Rheological properties of rennet-induced skim milk  
973 gels. 4. The effect of pH and NaCl, *Netherland Milk and Dairy Journal*, 43, 17–34.



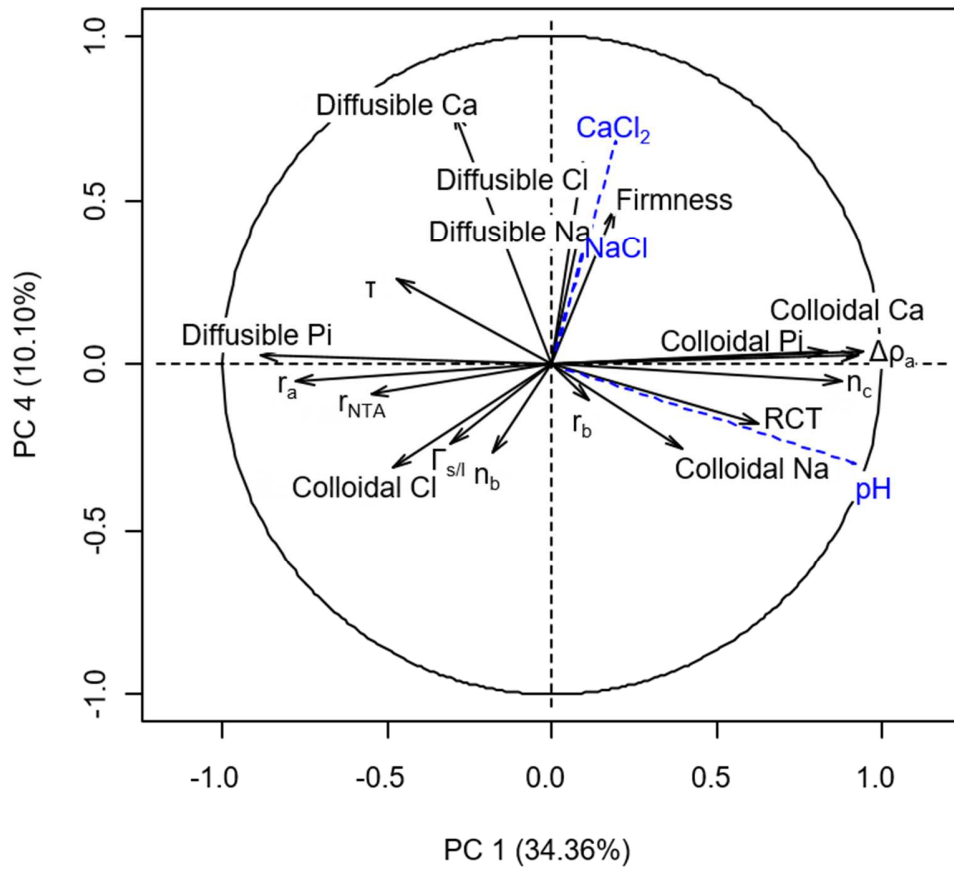
**A.**



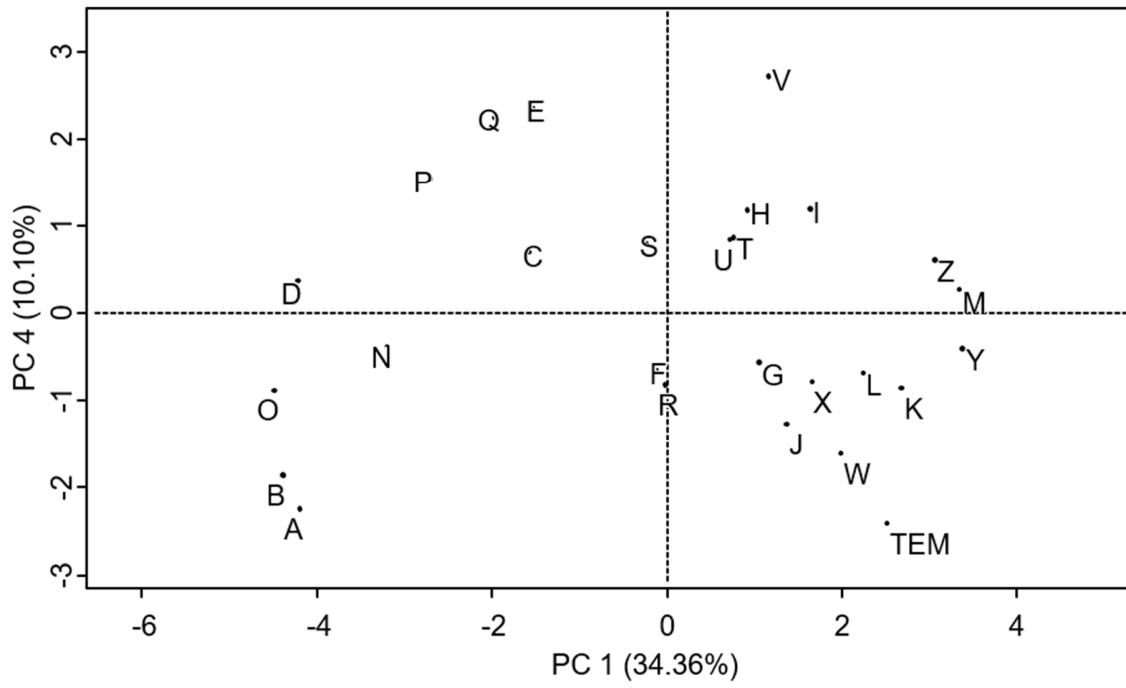
**B.**



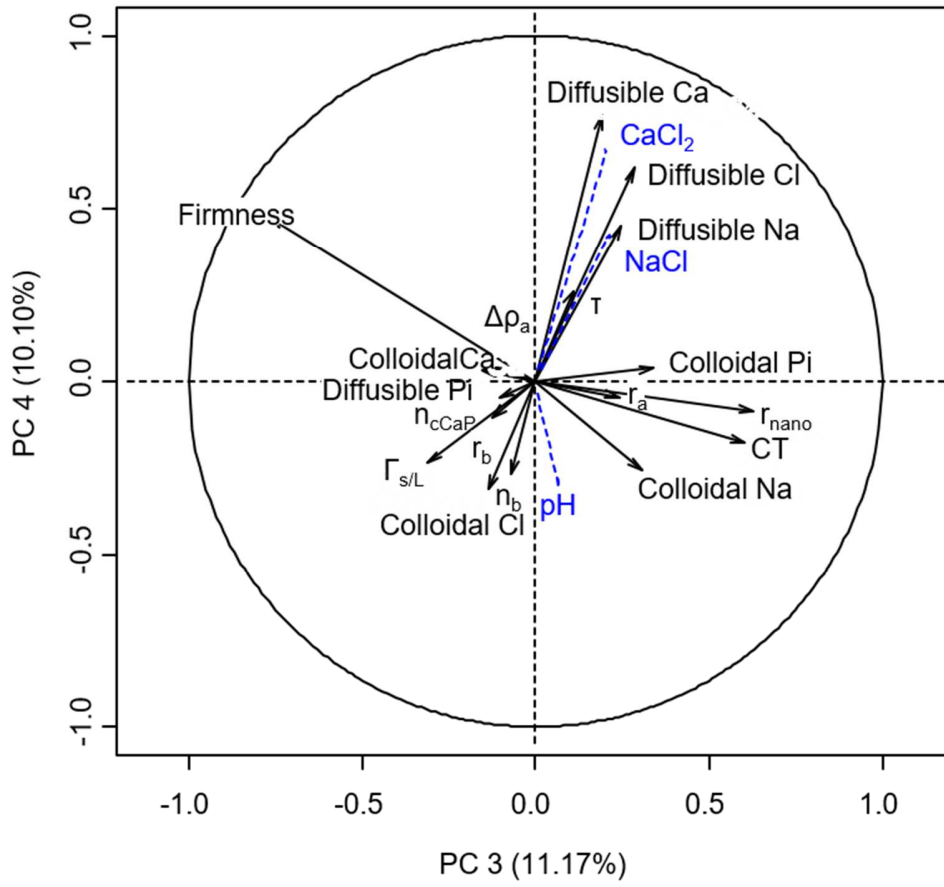
**A.**

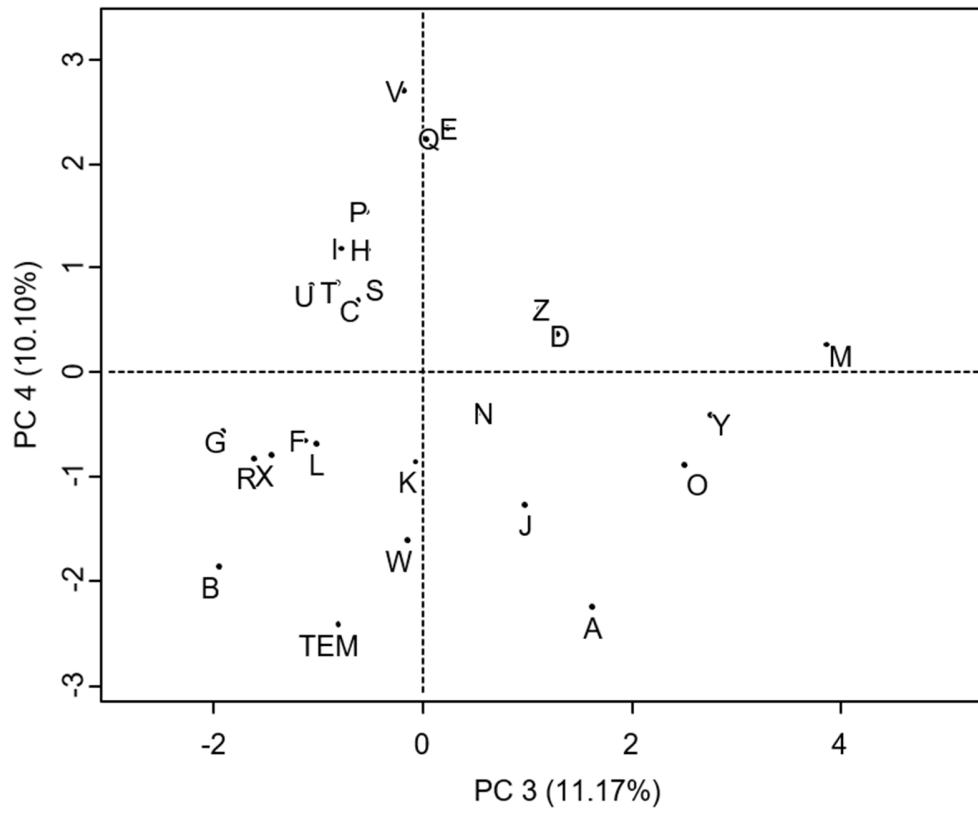


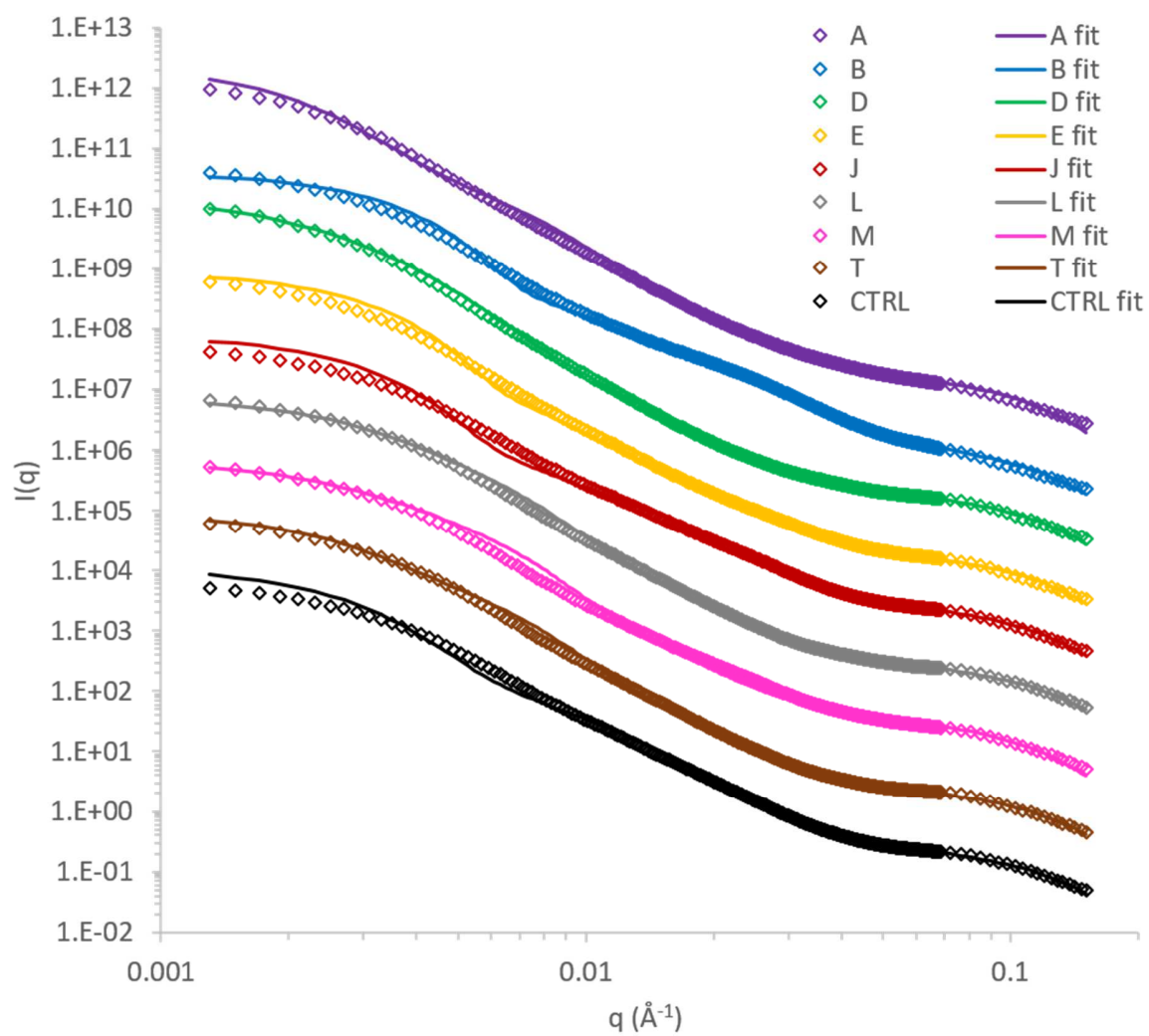
**B.**

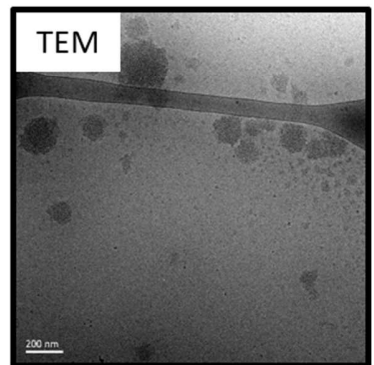
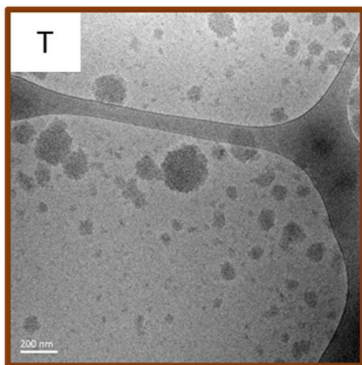
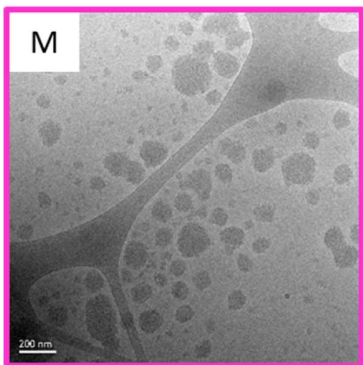
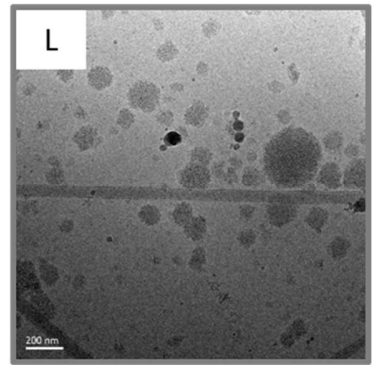
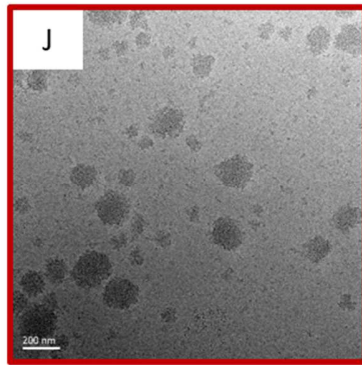
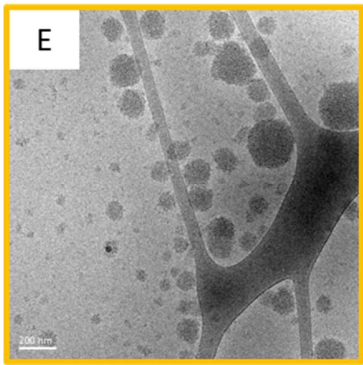
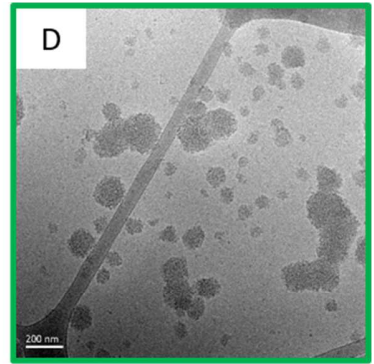
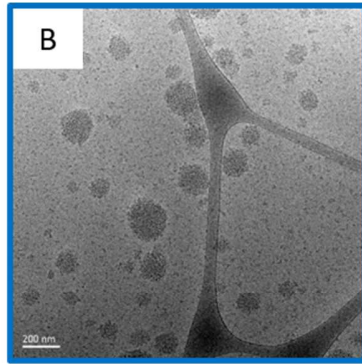
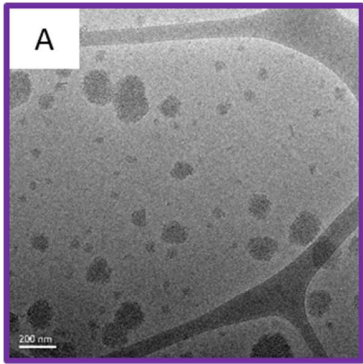


**A.**

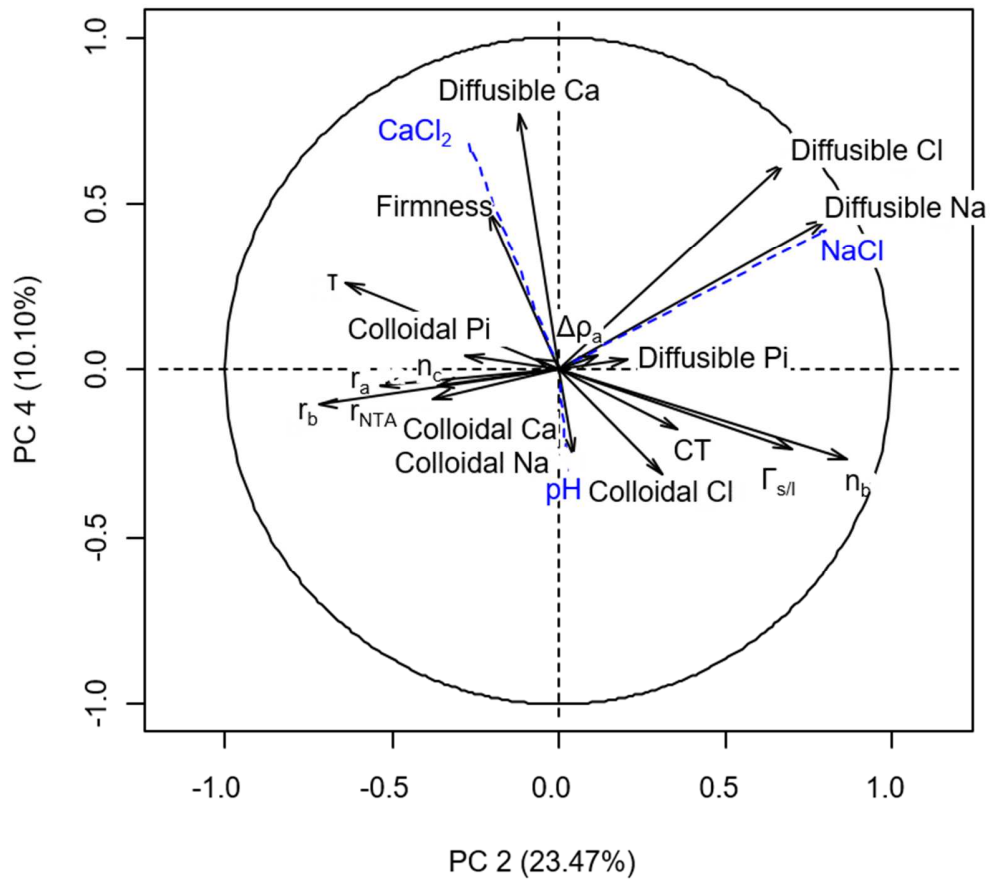




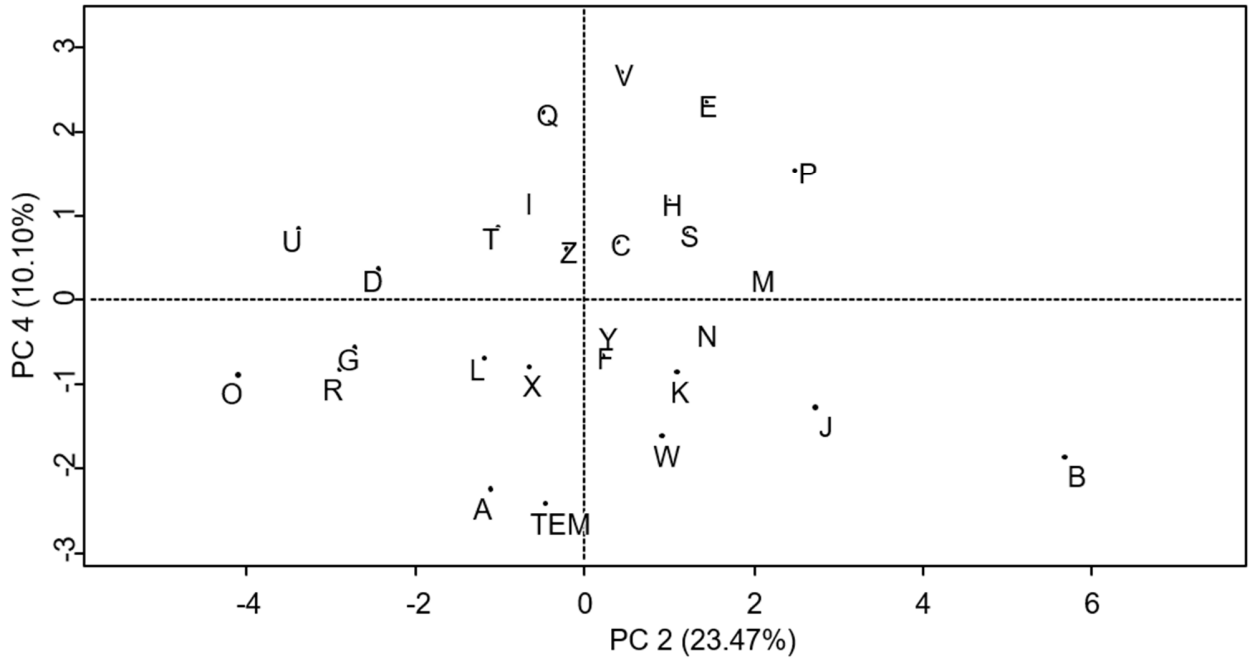


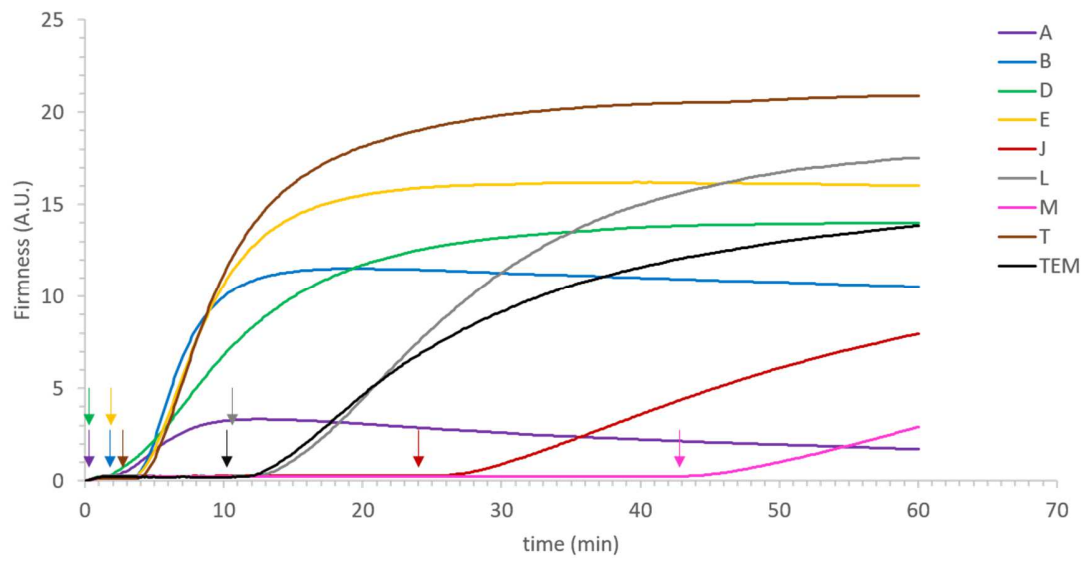


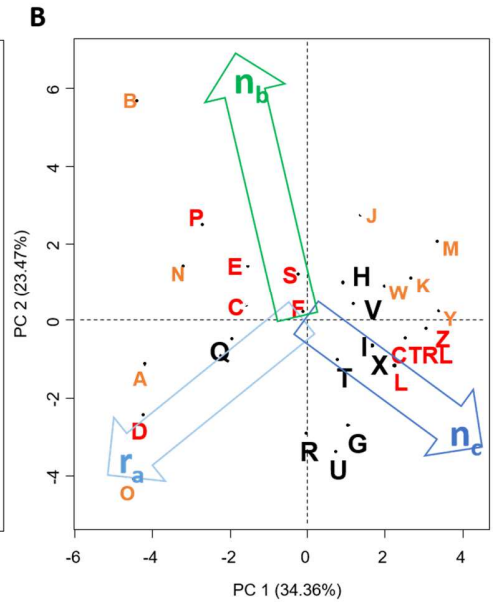
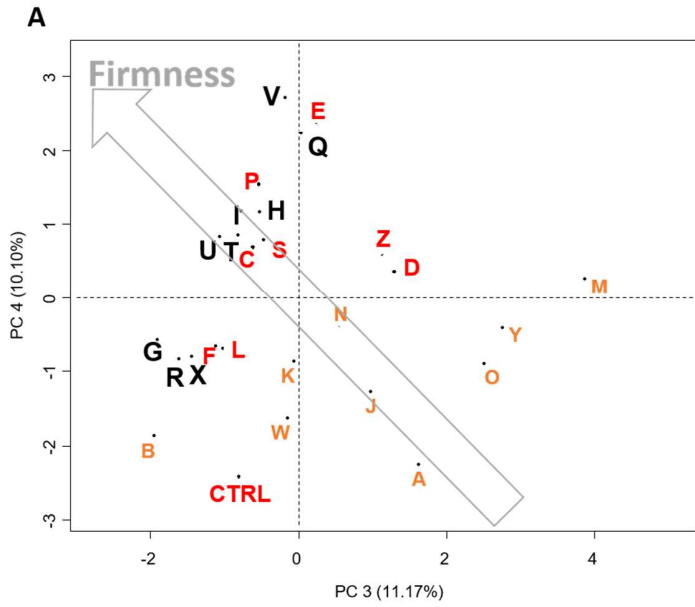
**A.**



**B.**







	Diffusible Ca (mmol kg <sup>-1</sup> )	Colloidal Ca (mmol kg <sup>-1</sup> )	Diffusible Na (mmol kg <sup>-1</sup> )	Colloidal Na (mmol kg <sup>-1</sup> )	Diffusible Cl (mmol kg <sup>-1</sup> )	Colloidal Cl (mmol kg <sup>-1</sup> )	Diffusible Pi (mmol kg <sup>-1</sup> )	Colloidal Pi (mmol kg <sup>-1</sup> )
Full experimental plan - 27 suspensions								
Average	12.4	14.8	64.8	0.2	67.4	0.5	2.4	4.6
SD	6.0	4.3	45.5	0.5	45.7	1.4	1.3	1.3
RSD (%)	48.2	29.2	70.3	300.9	67.8	287.6	55.1	28.1
minimum	2.1	3.6	6.7	0.0	0.0	0.0	0.0	1.9
maximum	22.9	20.2	135.6	2.2	138.0	6.2	5.0	7.2
Selected individual suspensions								
A	9.6	8.2	8.9	0.0	2.2	1.6	3.8	3.3
B	11.0	8.8	114.4	0.0	102.7	6.2	4.8	1.9
D	20.1	12.0	24.0	0.0	26.9	3.3	2.9	3.5
E	22.8	12.3	121.7	0.0	130.7	0.0	3.4	3.5
J	3.5	15.8	120.2	0.0	94.4	0.0	1.7	4.9
L	14.7	20.2	10.5	0.0	17.9	1.8	0.8	5.4
M	16.3	18.8	135.6	0.0	129.4	0.0	0.0	6.9
T	11.5	15.8	65.4	0.0	69.2	0.0	2.3	5.0
CTRL	2.1	18.0	6.7	0.8	0.0	0.0	1.6	4.9

	Turbidimetry	NTA	SAXS							Cryo TEM
	$\tau$ ( $\text{cm}^{-1}$ )	$r_{\text{NTA}}$ (nm)	$\Delta\rho_a$ ( $\text{e} \cdot \text{A}^{-3}$ )	$r_a$ (nm)	$r_b$ (nm)	$r_c$ (nm)	$n_b$	$n_{\text{CaP}}$	$n_{\text{cPI}}$	$\Gamma_{s/l}$
Full experimental design - 27 suspensions										
Average	21.2	61.0	0.015	45.6	10.7	1.6	3.3	171.5	318.9	8.5
SD	6.8	5.5	0.002	4.2	4.2	0.0	2.8	54.0	100.4	7.8
RSD (%)	32.1	9.0	13.5	9.3	38.9	3.1	84.1	31.5	31.5	91.0
minimum	12.6	53.8	0.010	41.5	6.1	1.5	0.2	75.3	140.0	0.9
maximum	43.8	74.8	0.018	58.1	21.9	1.7	13.3	243.7	453.3	35.6
Selected individual suspensions										
A	21.4	70.8	0.011	54.7	7.6	1.7	2.1	87.0	161.9	6.7
B	14.6	53.8	0.012	45.5	6.9	1.6	13.3	75.3	140.0	35.6
D	43.8	73.4	0.012	54.5	6.1	1.6	1.6	127.4	236.9	3.0
E	18.0	59.6	0.014	46.4	7.6	1.6	4.0	121.6	226.2	6.2
J	14.0	59.3	0.016	41.8	8.7	1.6	6.6	174.2	324.0	16.8
L	13.8	59.8	0.018	43.5	12.8	1.6	1.2	231.7	431.0	6.7
M	12.6	61.8	0.017	42.3	8.3	1.6	5.1	202.6	376.9	1.7
T	24.5	62.1	0.017	44.3	12.2	1.6	1.3	203.1	377.8	6.0
CTRL	15.7	57.0	0.018	41.5	10.1	1.5	4.0	228.0	424.1	4.6

	Firmness (A.U.)	RCT (min)
full experimental design - 27 suspensions		
Average	14.9	8.6
SD	5.1	9.8
RSD (%)	34.0	113.5
minimum	3.0	1.1
maximum	20.9	42.4
Selected individual suspensions		
A	3.3	1.4
B	11.5	2.9
D	14.0	1.4
E	16.2	2.9
J	8.0	24.6
L	17.5	11.2
M	3.0	42.4
T	20.9	3.4
CTRL	13.9	11.0

**Table 1: Distribution of the mineral salts in the suspensions.** Colloidal concentrations were determined by subtracting the concentration of diffusible ions from the concentration of total ions. Average, standard deviation (SD), relative standard deviation (RSD), minimum and maximum values were determined on the complete set of 27 samples.

	Diffusible Ca (mmol kg <sup>-1</sup> )	Colloidal Ca (mmol kg <sup>-1</sup> )	Diffusible Na (mmol kg <sup>-1</sup> )	Colloidal Na (mmol kg <sup>-1</sup> )	Diffusible Cl (mmol kg <sup>-1</sup> )	Colloidal Cl (mmol kg <sup>-1</sup> )	Diffusible Pi (mmol kg <sup>-1</sup> )	Colloidal Pi (mmol kg <sup>-1</sup> )
Full experimental plan - 27 suspensions								
Average	12.4	14.8	64.8	0.2	67.4	0.5	2.4	4.6
SD	6.0	4.3	45.5	0.5	45.7	1.4	1.3	1.3
RSD (%)	48.2	29.2	70.3	300.9	67.8	287.6	55.1	28.1
minimum	2.1	3.6	6.7	0.0	0.0	0.0	0.0	1.9
maximum	22.9	20.2	135.6	2.2	138.0	6.2	5.0	7.2
Selected individual suspensions								
A	9.6	8.2	8.9	0.0	2.2	1.6	3.8	3.3
B	11.0	8.8	114.4	0.0	102.7	6.2	4.8	1.9
D	20.1	12.0	24.0	0.0	26.9	3.3	2.9	3.5
E	22.8	12.3	121.7	0.0	130.7	0.0	3.4	3.5
J	3.5	15.8	120.2	0.0	94.4	0.0	1.7	4.9
L	14.7	20.2	10.5	0.0	17.9	1.8	0.8	5.4
M	16.3	18.8	135.6	0.0	129.4	0.0	0.0	6.9
T	11.5	15.8	65.4	0.0	69.2	0.0	2.3	5.0
CTRL	2.1	18.0	6.7	0.8	0.0	0.0	1.6	4.9

**Table 2: Size-related parameters determined by different analytical methods including Turbidimetry, NTA, SAXS and Cryo-TEM.** Average, standard deviation (SD), relative standard deviation (RSD), minimum and maximum values were determined on the complete set of 27 samples. ncCaP and ncPI correspond to the number of C scatterers per casein micelle, in the case where these scatterers are considered as CaP nanoclusters or protein Inhomogeneities, respectively.

	Turbidimetry	NTA	SAXS							Cryo TEM
	$\tau$ ( $\text{cm}^{-1}$ )	$r_{\text{NTA}}$ (nm)	$\Delta\rho_a$ ( $\text{e}^- \cdot \text{Å}^{-3}$ )	$r_a$ (nm)	$r_b$ (nm)	$r_c$ (nm)	$n_b$	$n_{\text{cCaP}}$	$n_{\text{cPI}}$	$\Gamma_{s/l}$
Full experimental design - 27 suspensions										
Average	21.2	61.0	0.015	45.6	10.7	1.6	3.3	171.5	318.9	8.5
SD	6.8	5.5	0.002	4.2	4.2	0.0	2.8	54.0	100.4	7.8
RSD (%)	32.1	9.0	13.5	9.3	38.9	3.1	84.1	31.5	31.5	91.0
minimum	12.6	53.8	0.010	41.5	6.1	1.5	0.2	75.3	140.0	0.9
maximum	43.8	74.8	0.018	58.1	21.9	1.7	13.3	243.7	453.3	35.6
Selected individual suspensions										
A	21.4	70.8	0.011	54.7	7.6	1.7	2.1	87.0	161.9	6.7
B	14.6	53.8	0.012	45.5	6.9	1.6	13.3	75.3	140.0	35.6
D	43.8	73.4	0.012	54.5	6.1	1.6	1.6	127.4	236.9	3.0
E	18.0	59.6	0.014	46.4	7.6	1.6	4.0	121.6	226.2	6.2
J	14.0	59.3	0.016	41.8	8.7	1.6	6.6	174.2	324.0	16.8
L	13.8	59.8	0.018	43.5	12.8	1.6	1.2	231.7	431.0	6.7
M	12.6	61.8	0.017	42.3	8.3	1.6	5.1	202.6	376.9	1.7
T	24.5	62.1	0.017	44.3	12.2	1.6	1.3	203.1	377.8	6.0
CTRL	15.7	57.0	0.018	41.5	10.1	1.5	4.0	228.0	424.1	4.6

**Table 3: Rennet coagulation properties of Firmness and Rennet Coagulation Time (RCT).** Average, standard deviation (SD), relative standard deviation (RSD), minimum and maximum values were determined on the complete set of 27 samples.

	Firmness (A.U.)	RCT (min)
full experimental design - 27 suspensions		
Average	14.9	8.6
SD	5.1	9.8
RSD (%)	34.0	113.5
minimum	3.0	1.1
maximum	20.9	42.4
Selected individual suspensions		
A	3.3	1.4
B	11.5	2.9
D	14.0	1.4
E	16.2	2.9
J	8.0	24.6
L	17.5	11.2
M	3.0	42.4
T	20.9	3.4
CTRL	13.9	11.0

